Fluid Phase Equilibria 572 (2023) 113833

Contents lists available at ScienceDirect

Fluid Phase Equilibria

journal homepage: www.sciencedirect.com/journal/fluid-phase-equilibria

Data science for thermodynamic modeling: Case study for ionic liquid and hydrofluorocarbon refrigerant mixtures

Bridgette J. Befort, Alejandro Garciadiego, Jialu Wang, Ke Wang, Gabriela Franco, Edward J. Maginn, Alexander W. Dowling *

Department of Chemical and Biomolecular Engineering, University of Notre Dame, Notre Dame, IN 46556, United States

ARTICLE INFO

Dataset link: https://github.com/dowlinglab/HFC-IL-thermodynamic-model-selection

Keywords:
Data science
Model selection
Model-based design of experiments
Nonlinear regression
Fisher information matrix

ABSTRACT

The sustainable phaseout of high global warming potential hydrofluorocarbon (HFC) refrigerant mixtures requires novel solvents, such as ionic liquids (ILs), for new HFC reuse and recycle technologies. Accurate, predictive, and interpretable thermodynamic models for HFC/IL mixtures are essential for multiscale design schemes aiding this phaseout. Still, there is limited guidance regarding the best thermodynamic model for an HFC/IL system. We propose a rigorous thermodynamic model selection and analysis workflow for HFC/IL mixtures which harnesses data science tools – visualization, nonlinear regression, Akaike information criteria, Fischer information matrix (FIM)-based identifiability and uncertainty analyses, and model-based design of experiments methods – to evaluate the accuracy, predictive capability, and interpretability of a thermodynamic model. The open-source IDAES™ platform facilitates training and comparison of sixteen candidate HFC/IL thermodynamic models, including two cubic equations of state, Peng–Robinson and Soave–Redlich–Kwong, and eight variations on temperature dependence within a classical van der Waals mixing rule. We apply this analysis to models for three HFC/IL systems: HFC-32/[emim][TF_2N], HFC-125/[emim][TF_2N], and HFC-32/[bmim][PF_6]. For these mixtures, we observe that models with a temperature dependent mixing rule are consistently ranked higher by Akaike information criteria for model selection. However, these models may still have high parameter uncertainty and correlation, indicating that data at multiple temperatures should be obtained. This result differs from the current practice of generating single isotherm dataset for most new HFC/IL mixtures. Additionally, we find that the most valuable experiments are taken at the bounds of composition, temperature (e.g., 273 and 348 K), and pressure (e.g., 1 MPa) measurements. This analysis guides data generation efforts, showing that optimally selected measurements across multiple temperatures are adequate for regressing thermodynamic models for multiscale process design.

1. Introduction

1.1. Novel technology is needed for sustainable implementation of hydrofluorocarbon refrigerant phaseout

The phaseout of high global warming potential (GWP)[1] refrigerants, comprised of low and high GWP hydrofluorocarbons (HFCs) [4–6], has been recently mandated by US law [7,8] and international agreements [9,10]. For example, the commonly used refrigerant R-410a (GWP = 2088), comprised of an equimass mixture of the relatively low GWP HFC-32 (difluoromethane, GWP = 674) and the high GWP HFC-125 (pentafluoroethane, GWP = 3500), is scheduled for phaseout [11]. These HFC refrigerants are high-value chemicals. For example, the one hundred million kilograms of HFC-32 in circulation are worth five hundred million US dollars [12]. Additionally, the US Environmental Protection Agency estimates the societal benefit of this phaseout is seventeen billion US dollars by 2036, the goal year for 85% HFC reduction under the Kigali Amendment to the Montreal Protocol [8–10]. Furthermore, HFC phaseout provides opportunities for energy-saving innovation in refrigeration technology and the ensuing reduction in other harmful emissions, such as sulfur dioxide, nitrogen oxides, and fine particle matter [13].

While illegal venting or expensive incineration are the simplest disposal options, neither recoup the full HFC phaseout environmental or economic benefits. Instead, HFC refrigerant mixtures must be separated into their low-GWP HFC components, which can be reused [12,14], and

* Corresponding author.
E-mail address: adowling@nd.edu (A.W. Dowling).

[1] The GWP of a substance is calculated relative to GWP of carbon dioxide which is defined as one. High GWPs of HFCs are the result of their long atmospheric lifetimes and ability to absorb infrared radiation [1–3].

https://doi.org/10.1016/j.fluid.2023.113833
Received 16 January 2023; Received in revised form 24 April 2023; Accepted 27 April 2023
Available online 6 May 2023

their high-GWP HFC components, which can be recycled as feed stocks for other chemical products or next generation refrigerants [5,15–19]. Complicating this solution is the azeotropic nature of the HFC refrigerant mixtures, which leads to exorbitant separation energy and engineering costs [6,20].

Novel energy efficient separation systems, such as extractive distillation [21,22], adsorption [19,23–28], and membrane separation [29–33], can facilitate HFC phaseout, but require the development of solvents or separation materials. Ionic liquids (ILs) are salts that are liquids below 100 °C with essentially no vapor pressure that could potentially be used to break azeotropes [34–39]. However, millions of ILs exist, each with unique separation properties [39–41]. This complexity makes IL-enabled HFC separation schemes an excellent case study for integrated multi-scale computer-aided molecular and process design (CAM/PD) paradigms [42–47].

1.2. Numerous thermodynamic models are available for HFC/IL systems

Thermodynamic models predict thermophysical properties of pure substances and their mixtures. They translate discrete experimental data into continuous functions which can be used in process design and optimization, making them essential to CAM/PD [48–50]. Thermodynamic models are often calibrated using solubility data, e.g., liquid phase composition versus pressure, of mixtures of HFCs and ILs at various temperatures. Asensio-Delgado et al., provide an excellent review of phase equilibrium models for HFC/IL systems [34], categorized as activity coefficient models [51–53], such as Margules, Wilson, and non-random two-liquid (NRTL), cubic equations of state (EoS) [54–64], including van der Waals (vdW), Peng–Robinson (PR), and Redlich–Kwong (RK), statistical associating fluid theory (SAFT)-derived EoS [18,65,66], predictive, e.g. COSMO-RS [66,67], more complicated EoS available in process simulators, such as AspenPlus [68,69], molecular models [70] and machine learning models [34,71–73].

Often, authors of HFC/IL mixture studies, ourselves included, make *ad hoc* decisions when selecting a thermodynamic model guided by prior experience, preference, or convenience. For example, we have followed the path of Shiflett and Yokozeki [60], who observed in the early 2000s that cubic EoS used with the specially derived refrigerant–lubricant mixing rules provided good fits of the HFC/IL mixtures [74]. More recently, we used a five parameter cubic EoS with the refrigerant–lubricant mixing rules to model the solubility of HFC-32 and HFC-125 in six ILs [61]. However, a parameter uncertainty analysis identified parameter correlation, suggesting the possibility of a similarly accurate, reduced parameter thermodynamic model. In a subsequent study, we utilized a two parameter PR EoS with classical vdW mixing rules for four new HFC/IL systems [62].

1.3. We propose a systematic method for thermodynamic model selection demonstrated for HFC/IL systems

Thermodynamic model accuracy and uncertainty are significant limiting factors of CAM/PD [75,76], making the current approach to HFC/IL thermodynamic model selection problematic. Thermodynamic models must be accurate, predictive, parsimonious, i.e., not over fit, and informative, i.e., physically interpretable and justified by the data. Understanding and balancing these model characteristics enables uncertainty quantification and propagation to the molecular and process design calculations and decisions [77].

Heuristics predominantly justify thermodynamic model selection. Heuristics are based on fundamentals of the system of interest, including the properties of interest (e.g., thermodynamic, transport properties) and available data; the composition and molecular interactions (e.g., presence of polarity); and the process pressures and temperatures of interest, particularly with respect to system phase behavior [48,78,79]. Process simulators, such as AspenPlus, [80] contain libraries of thermodynamic models and regressed parameters for various systems, helping users apply heuristics to make informed modeling choices [81]. Once a model is identified with heuristics, it can be verified by evaluating its ability to reproduce binary phase diagrams in a process simulator, ternary phase diagrams, or experimental data [82].

We argue that the field of data science, which encompasses data curation, mining, and management, visualization, statistical inference, machine learning and artificial intelligence paradigms, provides a more principled framework for thermodynamic model selection than heuristics [83]. In particular, statistical methods can help balance model accuracy, predictiveness, and interpretability, while managing the bias versus variance trade-offs (e.g., over and underfit models, extrapolation) [84,85]. Data science applies to almost any data-rich field, including chemical engineering, where it is transforming traditional understanding of chemical processes on molecular to systems scales [83,86–88], including within CAM/PD frameworks [89,90].

Thus, this paper has two primary contributions. First, we propose a general workflow that harnesses data science tools to systematically evaluate, select, and analyze thermodynamic models for any mixture. Second, we apply this workflow to identify accurate, predictive, and informative thermodynamic models for three HFC/IL systems. The ionic liquids are comprised of two different cations, 1-ethyl-3-methylimidazolium (emim) and 1-n-butyl-3-methylimidazolium (bmim). These are paired with two different anions, hexafluorophosphate (PF_6) and bis(trifluoromethylsulfonyl)imide (TF_2N). The systems we investigated are HFC-32/[emim][TF_2N], HFC-125/[emim][TF_2N], and HFC-32/[bmim][PF_6]. As part of this analysis, we provide guidance to data generating collaborators on the most informative measurements to minimize the use of experimental resources. The remainder of this paper is organized as follows: in the Methods section, we review the workflow in generic terms, showcasing accessible data science tools for rigorous model selection and analysis. Then we apply this workflow to a library of candidate models for the HFC/IL mixtures, presenting key HFC/IL system insights. We conclude with recommendations and open questions for the HFC/IL thermodynamic modeling and data generation communities. Appendix A lists the abbreviations used throughout the paper in Table 10.

2. Methods

Fig. 1 shows our proposed data science workflow for rigorous thermodynamic model selection and analysis. We start with gathering thermophysical property data and postulating a library of candidate thermodynamic models. In Step 1, each model's parameters are estimated. In Step 2, a regressed model's fit is visualized and its error is quantified. Step 3 uses a model's error to rank the candidate models via Akaike information criterion (AIC). Step 4 includes computing the top AIC-ranked model's Fischer Information Matrix (FIM) and performing identifiability, uncertainty, and optimality criteria analyses. Finally, in Step 5, the FIM is used in model-based design of experiments (MBDoE) calculations to suggest new, informative measurements to data generating collaborators. This workflow is enabled by the open-source Institute for the Design of Advanced Energy Systems (IDAES™) Integrated Platform [91] and the Pyomo Python library [92,93]. These open-source packages enable transferability to various chemical systems and validation, reproducibility, and accountability. Additionally, IDAES provides opportunities to develop and explore the impacts of variations on traditional thermodynamic models, e.g., cubic EoS and mixing rules, and provides access to advanced data analysis methods (e.g., regression, MBDoE) and state-of-the-art optimization algorithms.

2.1. Step 1: Regress models

$$y_i = f(\mathbf{x}_i, \boldsymbol{\theta}) + \epsilon_i, \quad \epsilon_i \sim \mathcal{N}(0, \sigma_\epsilon^2) \tag{1}$$

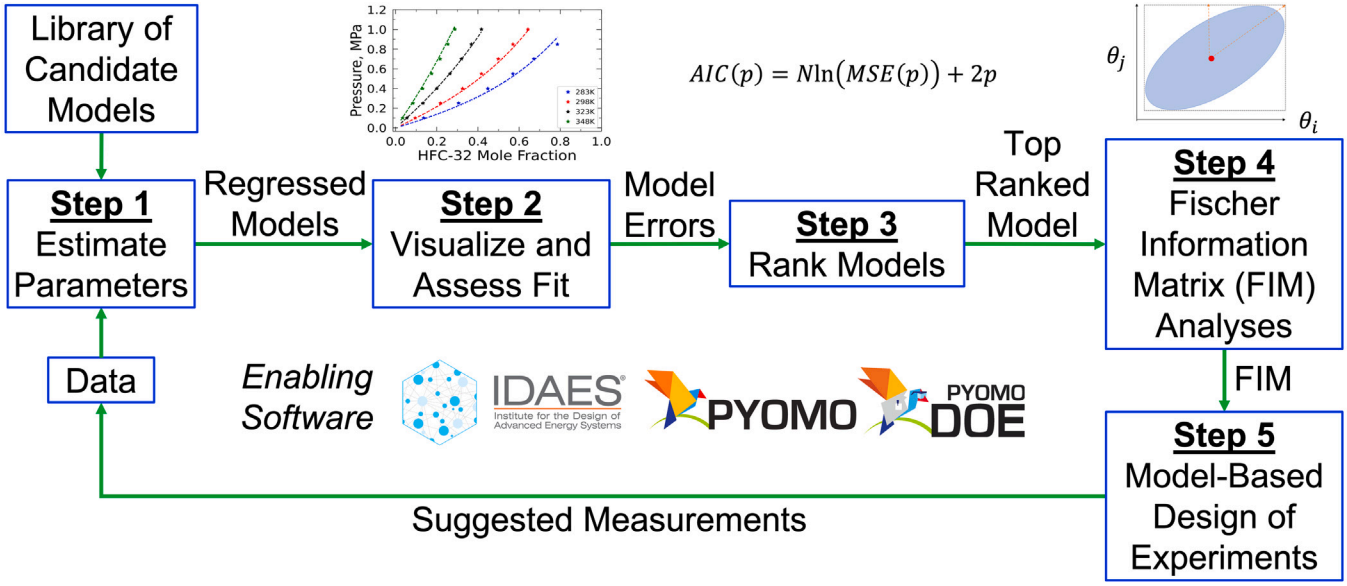

Fig. 1. Proposed data science enabled workflow for rigorous thermodynamic model selection and analysis.

For the general model shown in Eq. (1) the observation, y_i, are a function of inputs, $\mathbf{x}_i$, regressed parameters, $\theta \in \mathbb{R}^p$, and independent and identically normally distributed (mean zero, standard deviation σ_ϵ) observation error, ϵ. The model parameters are estimated from the data via least-squares nonlinear regression:

$$\hat{\theta} = \underset{\underline{\theta} \le \theta \le \bar{\theta}}{\arg\min}\, \Psi(\theta), \qquad \Psi(\theta) = \sum_{d=1}^{D}\left[\sum_{i=1}^{n_d}\left(y_{i,d} - f(\mathbf{x}_{i,d}, \theta)\right)^2\right] \tag{2}$$

In Eq. (2), Ψ is the least-squares loss function and $\hat{\theta}$ is the best fit estimate. Here we assume the dataset is partitioned into D experiments. Here n_d represents the number of observations in experiment d and $N = \sum_{d=1}^{D} n_d$ is the total number of observations. Alternatively, parameter estimation can be performed using maximum likelihood estimation (MLE) [94,95] or Bayesian model calibration [96].

2.2. Step 2: Assess quality of fit

Visualization demonstrates how well a model interpolates between its training data. Mean squared error (MSE) quantifies the quality of fit using the normalized error between the data and model predictions:

$$MSE = \frac{\Psi(\theta)}{N}, \qquad N = \sum_{d=1}^{D} n_d \tag{3}$$

MSE quantifies the average error per data point, making it a good metric to compare different models for single or multiple systems. In general, the lower a model's MSE value, the better the model's fit to the given data. Other fit metrics such as the sum of squared errors, root mean squared error, likelihood ratio test, or chi-square goodness of fit may be considered [97,98].

2.3. Step 3: Rank models

AIC is a mathematically rigorous method of model selection. AIC is a value assigned to rank a model based on its accuracy and parsimony, as quantified by its number of fitted parameters [97,99–101]. For a nonlinear, least-squares regression problem, the AIC value can be calculated based on the model's MSE, the number of parameters, p, and the total number of observations, N [99]:

$$AIC(p) = N\log_e(MSE) + 2p \tag{4}$$

AIC can rank a library of models: a low value of AIC indicates the model is less over fit, i.e., its complexity, p, is justified by its accuracy, MSE. The model with the lowest value of AIC is generally the model that should be *selected* from a library of candidate models.

The relative likelihood of a model, L_i, can be computed via:

$$L_i = \exp\left(\frac{AIC_{min} - AIC_i}{2}\right) \tag{5}$$

where AIC_{min} is the AIC value of the candidate model with the lowest AIC and AIC_i is the AIC of candidate model i. L_i is the relative probability of data given a hypothesized model. In other words, assuming a model i (functional form, regressed parameters, and error structure) is true, L_i quantifies the probability that the model i will reproduce the data relative to a reference model. Models with near-zero likelihood have a low probability of reproducing the data.

In contrast to the frequentist AIC model selection technique, Bayesian model selection is based on probabilistic fits of a model and can be used for pairwise model comparison via the Bayes factor and ranking multiple candidate models using Bayesian information criterion [97]. Bayesian methods allow modelers to account for experimental error by encoding a prior distribution of the data, generate probabilistic uncertainties of model parameters and predictions, and rank models while accounting for prediction uncertainties [84]. These methods have been shown to provide rigorous selection of thermodynamic models for such properties as viscosity [84], but require knowledge of probability distributions and Bayesian statistical tools to be implemented. At this time, Bayesian calibration and model selection remains computationally burdensome despite several recent research advances, but is a promising research direction [102]. We emphasize the proposed framework can be easily amended to use Bayesian statistical techniques.

2.4. Step 4: Fischer information matrix analyses

2.4.1. Compute the FIM

Using the best fit parameters, $\hat{\theta}$, and the corresponding objective value, Ψ, of the top AIC-ranked model, the first order sensitivity of the model, $f(\cdot,\cdot)$, with respect to $\hat{\theta}$ is computed. This matrix, $\boldsymbol{Q}$, of the first partial derivatives of the model with respect to the parameters is calculated via:

$$\boldsymbol{Q} = \begin{bmatrix} \frac{\partial f(x_1,\hat{\theta})}{\partial \hat{\theta}_1} & \cdots & \frac{\partial f(x_1,\hat{\theta})}{\partial \hat{\theta}_p} \\ \vdots & \ddots & \vdots \\ \frac{\partial f(x_N,\hat{\theta})}{\partial \hat{\theta}_1} & \cdots & \frac{\partial f(x_N,\hat{\theta})}{\partial \hat{\theta}_p} \end{bmatrix} \tag{6}$$

From $\boldsymbol{Q}$, the sensitivity of the objective, Ψ, to the parameters can be calculated via the Hessian matrix, $\boldsymbol{H}$:

$$\boldsymbol{H} = \begin{bmatrix} \frac{\partial^2 \Psi}{\partial \hat{\theta}_1^2} & \cdots & \frac{\partial^2 \Psi}{\partial \hat{\theta}_n \partial \hat{\theta}_1} \\ \vdots & \ddots & \vdots \\ \frac{\partial^2 \Psi}{\partial \hat{\theta}_1 \partial \hat{\theta}_p} & \cdots & \frac{\partial^2 \Psi}{\partial \hat{\theta}_p^2} \end{bmatrix} \approx \boldsymbol{Q}^T \boldsymbol{Q} \tag{7}$$

This approximation holds when the model residuals, i.e., errors, are small [95].

The covariance matrix quantifies how the measurement uncertainty, ϵ, shown in Eq. (1), propagates into uncertainty in the regressed parameters, $\hat{\boldsymbol{\theta}}$:

$$\boldsymbol{V}_{\hat{\theta}} \approx \sigma_\epsilon^2 \boldsymbol{H}^{-1} \approx \sigma_\epsilon^2 (\boldsymbol{Q}^T \boldsymbol{Q})^{-1} \tag{8}$$

Finally, the Fischer Information Matrix (FIM), $\boldsymbol{M}$, is approximately the inverse of the covariance matrix:

$$\boldsymbol{M} \approx \boldsymbol{V}_{\hat{\theta}}^{-1} \approx \frac{1}{\sigma_\epsilon^2} (\boldsymbol{Q}^T \boldsymbol{Q}) \tag{9}$$

The FIM represents the information about the parameters, $\hat{\theta}$, that is contained in the set of measurements used to fit the model [95,103,104]. A large FIM corresponds to a large amount of information within the data used to regress a given model [103]. If the model predictions, $f(\mathbf{x}_i, \boldsymbol{\theta})$ for all i, are insensitive to parameter θ_j, then this parameter can take multiple values without diminishing the best fit objective $\Psi(\cdot)$. If so, the sensitivity matrix, $\boldsymbol{Q}$, Hessian matrix, $\boldsymbol{H}$, covariance matrix, $\boldsymbol{V}_{\hat{\theta}}$, and the FIM, $\boldsymbol{M}$, are rank deficient. This indicates the dataset ($\mathbf{x}_i$, y_i for all i) cannot identify θ_j in the model, $f(\cdot,\cdot)$. Thus, there is large uncertainty in $\hat{\theta}_j$ and the corresponding elements of the covariance matrix, $\boldsymbol{V}_{\hat{\theta}}$. Consequently, if a rank deficient model is used in subsequent predictive calculations, e.g., process models, uncertainty associated with these calculations could be propagated from the model's uncertain parameters [95,104].

We note that the covariance matrix, $\boldsymbol{V}_{\hat{\theta}}$, and FIM, $\boldsymbol{M}$, are symmetric real-valued positive semi-definite matrices. As inverse matrices, $\boldsymbol{V}_{\hat{\theta}}$ and $\boldsymbol{M}$ have reciprocal eigenvalues, i.e., if λ_j is an eigenvalue of $\boldsymbol{V}_{\hat{\theta}}$, λ_j^{-1} is an eigenvalue of $\boldsymbol{M}$. Additionally, $\boldsymbol{V}_{\hat{\theta}}$ and $\boldsymbol{M}$ share eigenvectors. While the remaining analyses in this workflow could be performed with manipulations of either matrix, computing matrix inverses is slow and numerically unreliable for poorly conditioned systems. As such, in this work, we will perform subsequent analyses using the FIM, which we obtain via direct computation of $\boldsymbol{Q}$ using automatic differentiation and sensitivity analysis implemented in `Pyomo.DoE` [105].

2.4.2. Identifiability analysis

A model is said to be identifiable if there exists a single parameter vector, $\hat{\boldsymbol{\theta}}$, that corresponds to the minimum objective value $\Psi(\cdot)$ [95,104–107]. Likewise, if the objective function $\Psi(\cdot)$ is flat (i.e., almost no curvature indicated by near-zero eigenvalues) then the model predictions are insensitive to these parameters. Identifiability is an indicator of whether the model functional form and parameters are justified by the data. A model may be unidentifiable because of its functional form, a lack of experimental data, or poor numerical conditioning[108].

Non-unique parameters in an unidentifiable model are called *sloppy*. Sloppiness can be addressed by fixing parameters to specific values, i.e., removing them from the regression problem; adding more, and usually different, data to the model regression problem; or identifying a new model functional form. Sloppy parameters can be identified by eigendecomposition of the FIM. Eigenvalues of the FIM that are zero or near-zero suggest parameter sloppiness and indicate the model is near-singular. Additionally, a model is unidentifiable if its condition number, C_{FIM}, is greater than $\mathcal{O}(10^3)$ [105,109,110]:

$$C_{FIM} = \frac{\max \text{eig}(\boldsymbol{M})}{\min \text{eig}(\boldsymbol{M})} \geq \mathcal{O}(10^3) \tag{10}$$

Here, max eig($\boldsymbol{M}$) and min eig($\boldsymbol{M}$) refer to the largest and smallest eigenvalues, respectively, of a model's FIM. Sloppy parameters are identified in the eigenvectors which correspond to the sloppy eigenvalues. Often, an eigenvector points to a single direction, or parameter, which is sloppy. However, in some instances, the eigenvector shows the sloppiness is in the direction of a linear combination of the parameters [111,112].

2.4.3. Uncertainty analysis

Quantifying thermodynamic parameter uncertainties is essential to understand the technical risk at process scales in CAM/PD frameworks [64,112–117]. To date, we are unaware of any other considerations of uncertainty within IL-enabled HFC separations studies besides our own. We have explored parameter uncertainty using three methods: Monte Carlo (MC) uncertainty analyses [61,64], bootstrap methods [64], and covariance matrices [62]. MC uncertainty analyses account for experimental error by simulating the regression of a thermodynamic model thousands of times. In each regression, the original experimental data is varied within the bounds of the reported experimental error. See Morais et al., [61] and Garciadiego et al., [64] for a full description of this method. Bootstrap uncertainty methods involve leaving out a random subset of measurements from the fitting data set, regressing the parameters, and repeating this procedure multiple times. Then, the uncertainties or variations within the resulting parameter values are computed [64]. These small differences in data lead to variations, or corresponding uncertainties, within fitted parameter values. For both the MC and bootstrap methods, these parameter uncertainties are automatically used in process calculations to obtain process variable uncertainties. MC methods explicitly add measurement error from a specified probability distribution, whereas the bootstrap and covariance methods assume the error from the distribution of the data (typically a normal distribution).

The covariance matrix, as defined in Eq. (8), describes the variance of an individual model parameter and the co-varying relationship between two individual parameters. Covariance is defined as:

$$\boldsymbol{V}_{\hat{\theta}} = \begin{bmatrix} \sigma_{11}^2 & \cdots & \sigma_{1p}^2 \\ \vdots & \ddots & \vdots \\ \sigma_{p1}^2 & \cdots & \sigma_{pp}^2 \end{bmatrix} \tag{11}$$

Here, σ_{ii} is a parameter's variance and σ_{ij} represents the covariance between parameters i and j. These parameter uncertainties can be propagated to a model, $f(\cdot,\cdot)$, e.g., a thermodynamic model, that is a function of the parameters, $\hat{\boldsymbol{\theta}}$, using a first order error propagation formula:

$$\sigma_f^2 \approx \boldsymbol{Q}^T \boldsymbol{V}_{\hat{\theta}} \boldsymbol{Q} + \sigma_\epsilon^2 \tag{12}$$

The term σ_ϵ^2 accounts for observation error for the new experiment and may be omitted for process design calculations.

2.4.4. Optimality analysis

In MBDoE, alphabet design criteria, such as A-, D-, and E-optimality, summarized in Table 1, convert the FIM into a scalar value [105]. Geometrically, these criteria quantify features of a parameter's confidence ellipse. Mathematically, the confidence ellipse is defined by the eigendecomposition of the FIM. The FIM's eigenvectors are the directions of the axes of the ellipse for a given parameter, while the corresponding eigenvalues define the length or magnitude of the ellipse axes. The alphabet design criteria operate on the eigendecomposition results to increase the information content of a model by decreasing the uncertainty of its parameters, i.e., shrinking the confidence ellipse. For example, A-optimality minimizes the average variance of parameter estimates by minimizing the dimensions of the box which encloses the confidence ellipse of a given parameter. D-optimality minimizes the size, e.g., volume, of the confidence ellipse. E-optimality maximizes the smallest eigenvalue of the FIM, which in turn minimizes the size of the major axis of the confidence ellipse [105].

Table 1
Alphabet optimality criteria.

Criteria	Operation	Optimization
A	$\text{trace}(\boldsymbol{M}) = \sum_i \lambda_i$	$\max \text{trace}(\boldsymbol{M})$
D	$\det(\boldsymbol{M}) = \prod_i \lambda_i$	$\max \det(\boldsymbol{M})$
E	$\min\ \text{eig}(\boldsymbol{M}) = \min(\lambda_i)$	$\max \min \text{eig}(\boldsymbol{M})$

2.5. Step 5: Model-based design of experiments

Model-based design of experiments (MBDoE) is an iterative task [105] which guides the selection of experimental conditions to improve the precision of model parameters or discriminate between multiple candidate models or both. After measurements are gathered, a model is re-calibrated which results in new best fit parameters, $\hat{\theta}$, and a new FIM. With new experiments the FIM would contain more information, ideally making the parameters less sloppy and less uncertain. There are multiple types of MBDoE analyses, described below.

2.5.1. How much information does a data set contain?

Retrospective data analysis provides information about which data were most valuable. Each measurement in a data set has an individual FIM, $\boldsymbol{M}_i$, which quantifies the information experiment i contributes to a model. $\boldsymbol{M}_i$ are computed using Pyomo.DoE [105] and are summed to obtain the overall FIM for a model[2]:

$$\boldsymbol{M} = \sum_i \boldsymbol{M}_i \tag{13}$$

where $\boldsymbol{M}_i$ is computed with the sensitivity matrix $\boldsymbol{Q}_i$. The variation of magnitudes of the measurements and local parameter estimates can lead to ill-conditioned $\boldsymbol{M}_i$. One popular approach is scaling elements of $\boldsymbol{Q}$ by the parameter values:

$$Q_{i,j} \leftarrow \theta_j \cdot \frac{\partial f(x_i, \boldsymbol{\theta})}{\partial \theta_j}, \qquad \forall i \in \{1, \dots, N\}, \quad \forall j \in \{1, \dots, p\} \tag{14}$$

D-optimality analyses recommends new experiments to maximize the information content [118]. Wang et al. [118], describe an algorithm using D-optimality for determining the most informative experiments. This analysis provides information on the type of measurements, or the design space conditions, which contain the most information, elucidating the most valuable experiments for fitting a thermodynamic model.

2.5.2. What data are needed to discriminate between two models?

Model performance at out-of-sample conditions helps discriminate between two or more thermodynamic models. For two candidate models, $f_A(\xi, \hat{\theta}_A)$ and $f_B(\xi, \hat{\theta}_B)$, the Hunter–Reiner criterion identifies the conditions, ξ, which maximize the difference between their predictions for y [119]:

$$\max_{\xi} \quad \left(f_A(\xi, \hat{\theta}_A) - f_B(\xi, \hat{\theta}_B)\right)^2 \tag{15}$$

Alternative methods for model discrimination involve incorporating uncertainty information within the optimization problem [120, 121] in Eq. (15), developing a multi-objective formulation which allows for joint model discrimination and improvement of parameter confidence [122–125], and probabilistic analyses [126].

2.5.3. What new measurements contain the most information?

Design of experiments (DoE) analyses determine the conditions that optimize the amount of information contained within a measurement, often with the goal of reducing parameter uncertainty [105].

$$\begin{aligned} &\max_{\xi_L \le \xi \le \xi_U} \quad \zeta(\boldsymbol{M}(\hat{\theta}, \xi)) \\ &\text{such that} \quad \text{Eqs. (6)–(9)} \end{aligned} \tag{16}$$

[2] This formulation assumes that the measurement errors are uncorrelated.

Here, $\zeta : \mathbb{R}^{p \times p} \rightarrow \mathbb{R}$ are the A-, D-, or E-optimality metrics summarized in Table 1 and ξ represents the measurement conditions, i.e., MBDoE degrees of freedom. For low dimensional problems, performing a sensitivity analysis allows visualization of how each criterion changes with ξ which, in our opinion, is invaluable to build intuition and facilitate conversations with experimentally-focused collaborators; Pyomo.DoE facilitates this as well as numerically solving Eq. (16).

3. HFC/IL case study

Next, we describe specific considerations for applying the proposed workflow to HFC/IL systems.

We perform rigorous thermodynamic model analysis for three sets of HFC/IL solubility data, generated using an IGA gravimetric microbalance [61,62]:

1. Binary solubility of HFC-32 and [emim][TF_2N] at four temperatures: 283 K, 298 K, 323 K, and 348 K [127]. 27 total data points.
2. Binary solubility of HFC-125 and [emim][TF_2N] at four temperatures: 283 K, 298 K, 323 K, and 348 K [128]. 32 total data points.
3. Binary solubility of HFC-32 and [bmim][PF_6] at four temperatures: 283 K, 298 K, 323 K, and 348 K [129]. 31 total data points. The data for this system at 298 K was verified by Morais et al. [61].

These specific ILs were chosen because of the availability of high-quality solubility data in literature and recent process engineering analyses.

There are two major types of thermodynamic models, activity coefficient models and EoS, each of which can take many functional forms. Activity coefficient models express a solution's deviation from ideality while EoS represent relationships between state variables, i.e., temperature, pressure, volume, and composition, as continuous and differentiable functions [48]. Thermodynamic models contain parameters, often found in literature [61,62,130], which must be regressed using thermophysical data from the system of interest. Most thermodynamic models are nonlinear, and the resulting nonconvex parameter estimation problems require either multi-start initialization [64,131–135] or global optimization [136] to safeguard against multiple locally optimal solutions [95,104].

We now summarize the two cubic EoS, PR and Soave–Redlich–Kwong (SRK), and mixing rules explored in this work, enumerate a library of candidate models, and discuss the parameter estimation procedure. We study the PR and SRK models because they are widely used and popular in process simulators, such as AspenPlus [80], and are available in the open-source IDAES modeling framework.

The generic formula for a cubic EoS is:[137]

$$0 = Z^3 - (1 + B - uB)Z^2 + (A - uB - (u - w)B^2)Z - AB - wB^2 - 2B^3 \tag{17}$$

Here, Z represents the compressibility factor $Z = \frac{P\hat{V}}{RT}$, u and w are parameters describing the specific type of the EoS, e.g., PR or SRK, and:

$$A = \frac{a_m P}{R^2 T^2}, \tag{18}$$

$$B = \frac{b_m P}{RT}, \tag{19}$$

where, P is pressure, T is temperature, R is the gas constant, and a_m and b_m are mixture variables, which are calculating via the van der Waals mixing rule:

$$a_m = \sum_i \sum_j y_i y_j (a_i a_j)^{1/2} (1 - k_{i,j}), \tag{20}$$

$$b_m = \sum_j y_j b_j. \tag{21}$$

Table 2
Cubic EoS parameters.

Parameter	PR EoS	SRK EoS
u	2	1
w	−1	0
Ω_A	0.45724	0.42748
Ω_B	0.07780	0.08664
κ_j	$(1+(1-\sqrt{T_r})(0.37464+1.54226\omega_j-0.26992\omega_j^2))^2$	$(1+(1-\sqrt{T_r})(0.48+1.574\omega_j-0.176\omega_j^2))^2$

Here y_j is the mole fraction of each component, j, $k_{i,j}$ represents binary interaction parameters between components i and j, described more below, and a_j and b_j are pure component parameters:

$$a_j = \frac{\Omega_A R^2 T_{C,j}^2}{P_{C,j}} \kappa_j, \tag{22}$$

$$b_j = \frac{\Omega_B R T_{C,j}}{P_{C,j}}. \tag{23}$$

$P_{C,j}$ and $T_{C,j}$ are the critical temperature and pressure of component j. Ω_A, Ω_B, and κ_j are parameters specific to the EoS type and each component. These parameters are summarized for each cubic EoS in Table 2, where the reduced temperature is $T_r = T/T_C$ and ω_j is the acentric factor for component j.

Equivalently, the SRK EoS can be expressed to compute pressure:

$$P = \frac{RT}{V-b_m} - \frac{a_m}{V(V+b_m)} \tag{24}$$

The fugacity coefficient ϕ_j of component j in the mixture with the SRK EoS is calculated using:

$$\log\phi_j = \frac{b_j}{b_m}(Z-1) - \log(Z-B) - \frac{A}{B}\left(\frac{2}{a_m}\sum_j a_j - \frac{b_j}{b_m}\right)\log\left(1+\frac{B}{Z}\right) \tag{25}$$

Likewise, the PR EoS calculates pressure as:

$$P = \frac{RT}{V-b_m} - \frac{a_m}{V^2+2b_mV-b_m^2} \tag{26}$$

And, the fugacity coefficient ϕ_j of component j in the mixture with the PR EoS is calculated using:

$$\log\phi_j = \frac{b_j}{b_m}(Z-1) - \log(Z-B) - \frac{A}{2\sqrt{2}B}\left(\frac{2}{a_m}\sum_j a_j - \frac{b_j}{b_m}\right)\log\frac{Z+(\sqrt{2}+1)B}{Z-(\sqrt{2}-1)B} \tag{27}$$

We note that IL critical properties can only be estimated as pseudocritical points because their actual values are unknown. We previously [61,62] set the critical temperature to 1000 K, critical pressure to 2.5 MPa, and acentric factor to 0.5 for all ILs and follow the same conventions here [74,138,139]. In previous work [61,62], we showed the quality of fit is insensitive to these parameter choices.

Garciadiego et al., [64] previously showed that adding linear temperature dependence within the vdW mixing rule parameter improved the fit compared to a PR model without temperature dependence. Here, we expand upon this finding by considering four types of vdW mixing rule parameter temperature dependence: none, A, (original vdW mixing rule formulation); linear, B; quadratic, C; and order three polynomial, D.

$$k(T) = k_{ij,A} + k_{ij,B}T + k_{ij,C}T^2 + k_{ij,D}T^3 \tag{28}$$

Here, $k_{ii,X} = k_{jj,X} = 0$ with $X \in \{A,B,C,D\}$. Typically, symmetric binary interaction parameters $k_{ij,X} = k_{ji,X}$ are assumed. However, we found it numerically challenging to converge the parameter estimation problem when enforcing symmetric binary interaction parameters. By relaxing this assumption to use asymmetric binary interaction parameters $k_{ij,X} \neq k_{ji,X}$, we were able to more reliably converge the parameter estimation problem. As future work, the symmetric binary interaction parameters should be considered to reduce the number of fitted parameters.

Table 3
Library of postulated models for representing HFC/IL mixture properties.

Model	Temperature dependence	$k_{ij,A}$	$k_{ji,A}$	$k_{ij,B}$	$k_{ji,B}$	$k_{ij,C}$	$k_{ji,C}$	$k_{ij,D}$	$k_{ji,D}$
PR-1A	None	✓							
PR-1B	None		✓						
PR-2	None	✓	✓						
PR-3A	Linear	✓	✓	✓					
PR-3B	Linear	✓	✓		✓				
PR-4	Linear	✓	✓	✓	✓				
PR-6	Quadratic	✓	✓	✓	✓	✓	✓		
PR-8	Polynomial	✓	✓	✓	✓	✓	✓	✓	✓
SRK-1A	None	✓							
SRK-1B	None		✓						
SRK-2	None	✓	✓						
SRK-3A	Linear	✓	✓	✓					
SRK-3B	Linear	✓	✓		✓				
SRK-4	Linear	✓	✓	✓	✓				
SRK-6	Quadratic	✓	✓	✓	✓	✓	✓		
SRK-8	Polynomial	✓	✓	✓	✓	✓	✓	✓	✓

Evaluating thermodynamic model temperature dependence for HFC/IL systems is a unique contribution of this work. Recently, Privat and Jaubert [140] considered the theoretical interpretation of temperature-dependent binary interaction parameters. However, we are unaware of any other studies which systematically consider temperature-dependent binary interaction parameters for HFC/IL systems. In fact, HFC/IL experimental data are often only measured at room temperature, making temperature dependence analysis of the thermodynamic model impossible [61,62]. We note temperature dependence in the vdW mixing rule could be defined in multiple forms, e.g., as an inverse relationship, which is often included in process simulators [80]. To limit the candidate model library to a reasonable number of models (sixteen per system), we leave the exploration of other forms of temperature dependence to future work.

Finally, phase equilibrium between a vapor and liquid is calculated via:

$$(x_i\phi_i)^L = (y_i\phi_i)^V \tag{29}$$

Here, x_i and y_i are the mole fractions of the liquid and vapor, respectively, for a given component, and ϕ_i is the fugacity coefficient for component i for a specific phase, calculated via Eqs. (25) or (27). Because ILs have negligible vapor pressure, they do not exist in the vapor, i.e., $y_{HFC} = 1$. Thus, Eq. (29) becomes:

$$x_{HFC}\phi_{HFC}^L = \phi_{HFC}^V \tag{30}$$

Table 3 summarizes the library of candidate thermodynamic models. This library contains the two cubic EoS, PR and SRK, combined with temperature dependence variations in the classical vdW mixing rule, described in Eq. (28).

We used the parameter estimation formulation of Garciadiego et al. [64], to minimize the difference between experimental and model prediction pressures at a given temperature and composition:

$$\hat{k} = \arg\min_{k^l \le k \le k^u} \sum_{d=1}^{D}\left[\sum_{i=1}^{n_d}(\hat{P}(k,T_{i,d},x_{i,d}) - P_{i,d})^2\right] \tag{31}$$
$$\text{subject to} \quad \text{Eqs. (17)–(23), (28)}$$

Here $P_{i,d}$ is the experimental pressure, $T_{i,d}$ is the experimental temperature, and $x_{i,d}$ is the experimental composition of observation i

Table 4
Mean squared errors [MPa^2] of candidate models in model library for each HFC/IL system.

Model	HFC-32/ [emim][TF_2N]	HFC-125/ [emim][TF_2N]	HFC-32/ [bmim][PF_6]
PR-1A	1.26E−4	9.2E−6	1.82E−5
SRK-1A	1.39E−4	1.16E−5	2.31E−5
PR-1B	9.59E−4	8.09E−5	4.15E−4
SRK-1B	1.14E−3	2.50E−4	7.03E−4
PR-2	2.42E−5	5.82E−6	8.58E−6
SRK-2	2.99E−5	4.16E−6	1.11E−5
PR-3A	7.644E−6	3.68E−6	6.36E−6
SRK-3A	7.93E−6	3.71E−6	6.58E−6
PR-3B	2.41E−5	5.30E−6	8.30E−6
SRK-3B	2.95E−5	4.04E−6	1.16E−5
PR-4	1.67E−6	3.67E−6	4.34E−6
SRK-4	1.76E−6	3.71E−6	4.52E−6
PR-6	1.38E−6	3.54E−6	2.64E−6
SRK-6	1.42E−6	3.53E−6	2.68E−6
PR-8	1.32E−6	3.43E−6	2.36E−6
SRK-8	1.35E−6	3.43E−6	2.27E−6

Table 5
AIC ranking and relative likelihood for candidate models for the HFC-32/[emim][TF_2N] system.

Rank	Model	p	AIC	Likelihood, %
1	PR-6	6	−165.749	100
2	SRK-6	6	−165.055	70.7
3	PR-4	4	−164.664	58.1
4	SRK-4	4	−163.227	28.3
5	PR-8	8	−163.047	25.9
6	SRK-8	8	−162.320	18.0
7	PR-3A	3	−125.592	$O(10^{-7})$
8	SRK-3A	3	−124.603	$O(10^{-7})$
9	PR-2	2	−96.508	$O(10^{-7})$
10	PR-3B	3	−94.601	$O(10^{-7})$
11	SRK-2	2	−90.790	$O(10^{-7})$
12	SRK-3B	3	−89.102	$O(10^{-7})$
13	PR-1A	1	−53.919	$O(10^{-7})$
14	SRK-1A	1	−51.216	$O(10^{-7})$
15	PR-1B	1	0.860172	$O(10^{-7})$
16	SRK-1B	1	5.564	$O(10^{-7})$

in data set d. $\hat{P}$ is the model prediction of pressure at the given experimental temperature and composition and the set of binary interaction parameters, k. n_d is the number of data points in an individual data set d. There are D total number of data sets. Each HFC/IL system has four total data sets, one at each temperature.

This optimization problem is constrained by Eqs. (17)–(23) and (28), with specific parameters for the PR and SRK models described in Table 3. To estimate parameters, the model is formulated in Pyomo via `IDAES` (version: 1.13.0.dev0) and solved using the parmest package with the `IPOPT` [141] (version: 3.13.2) and `HSL (MA27)` [142] solvers. The set of binary interaction parameters, k, are bounded by $k^l = -20$ and $k^u = 20$.

Finally, the MSE is computed for each model via:

$$MSE = \frac{\sum_{d=1}^{D}\left[\sum_{i=1}^{n_d}(\hat{P}(k, T_{i,d}, x_{i,d}) - P_{i,d})^2\right]}{N} \tag{32}$$

For clarity, Eq. (1) is a general nonlinear calibration model, whereas Eqs. (26) (PR) and (24) (SRK) are the specific models considered here. The general parameter estimation optimization problem, Eq. (2), corresponds to Eq. (31). The generalized MSE equation, (3), corresponds to Eq. (32).

4. Results and discussion

We now analyze the results of applying the workflow in Fig. 1 to the three HFC/IL systems: HFC-32/[emim][TF_2N], HFC-125/[emim][TF_2N], and HFC-32/[bmim][PF_6].

4.1. Visualization provides an incomplete view of thermodynamic model regressions results

Fig. 2 shows each calibrated candidate model for the HFC-32/[emim][TF_2N] system. SI Figures SI1 and SI2 report similar results for the HFC-32/[bmim][PF_6] and HFC-125/[emim][TF_2N] systems. Moreover, SI Figures SI3 and SI4 are companion parity plots for Fig. 2. The four one parameter models, PR-1 A and PR-1B (a) and SRK-1 A and SRK-1B (b), have visually poor fits for all HFC/IL systems. The fits for the models with two or more parameters (plots c-h) are visually indistinguishable, making model selection via visualization alone impossible. These results raise a fundamental question of whether the data support the additional complexity of the models with more than two parameters.

Table 4 shows the MSE values for each candidate model for each HFC/IL system. For all three systems, the PR-8 and SRK-8 models (polynomial temperature dependence) have the lowest MSE values while the one parameter models give the worst fits, which is consistent with Fig. 2. There are two to three orders of magnitude difference between the MSEs of the one parameter and eight parameter models. Adding parameters to a model increases the optimization degrees of freedom and cannot increase the error objective, although the optimizer is free to set parameters to zero, which would result in a lower complexity model. We additionally observe that PR-1B and SRK-1B, the models in which only the $k_{IL,HFC,A}$ parameter is fit while the $k_{HFC,IL,A}$ parameter is fixed at zero, have the highest MSE values of all of the models, indicating that these models strongly depend on the presence of the $k_{HFC,IL,A}$ parameter.

This analysis, which is Step 2 of Fig. 1, shows that visualization and quality of fit metrics alone cannot discriminate between models, but can identify poorly performing models.

4.2. AIC rankings provide insight into the balance between model accuracy and parsimony

Tables 5–7 show the AIC values and relative likelihoods for the library of candidate models for each system.

HFC-32/[emim][TF_2N]

Table 5 shows the models for the HFC-32/[emim][TF_2N] system, ranked in order of lowest to highest AIC. The results are: PR-6, likelihood: 100%; SRK-6, likelihood: 70.7%; PR-4, likelihood: 58.1%; SRK-4, likelihood: 28.3%; PR-8, likelihood: 25.9%; and SRK-8, likelihood: 18.0%. The remainder of the models for this system have relative likelihoods that are essentially zero, i.e., on the order of 10^{-7} or smaller. A trade-off is observed between the quality of fit and parsimony between the six and eight parameter models. Although PR-8 and SRK-8 (which contain 8 fitted parameters) have lower MSE values than PR-6 and SRK-6 (which contain 6 fitted parameters), the contribution of their eight parameters makes their AIC values higher, decreasing the likelihood that they will best reproduce the data.

Based on AIC rank alone, PR-6 would be the model selected for the HFC-32/[emim][TF_2N] system. However, the top six models all have non-negligible likelihoods, resulting from very similar low MSE values. This suggests that none of these models are over fit and that they all are generally able to balance accuracy with parsimony, i.e., any of these top six models may justifiably reproduce the data.

HFC-125/[emim][TF_2N]

Table 6 shows all of the models except the one parameter models (PR-1 A, PR-1B, SRK-1 A, and SRK-1B) which have likelihoods greater than $O(10^{-3})$ for the HFC-125/[emim][TF_2N] system. PR-3 A (likelihood: 100%) is ranked highest, closely followed by SRK-3 A (likelihood: 88.0%). Rounding out the top five models are PR-4 (likelihood: 38.1%), SRK-2 (likelihood: 37.3%), and SRK-4 (likelihood: 32.4%). As with the

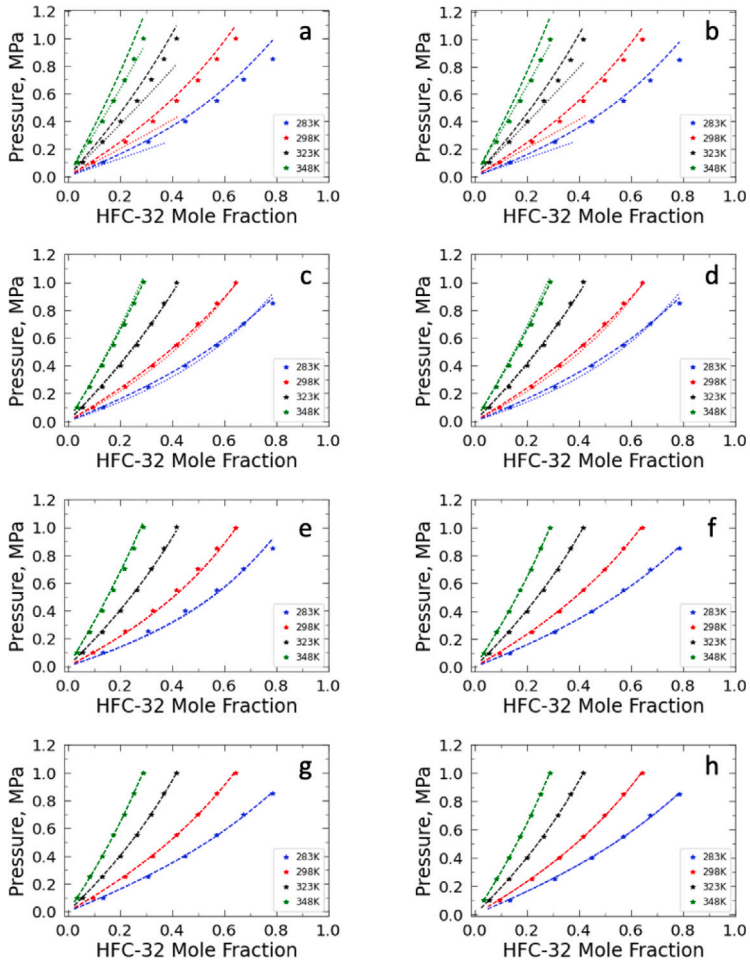

Fig. 2. Fits of the sixteen candidate models to HFC-32/[emim][TF_2N] solubility data [127]. Points are experimental data and lines are model fits. **Plot (a)** shows the fit for the PR-1 A [dashed] and the PR-1B [dotted] models. **Plot (b)** shows the fit for the SRK-1 A [dashed] and the SRK-1B [dotted] models. **Plot (c)** shows the fit for the P-3 A [dashed] and the PR-3B [dotted] models and **plot (d)** shows the fit for the SRK-3 A [dashed] and the SRK-3B [dotted] models. **Plots (e)–(h)** show the results of the PR [dashed] and SRK [dotted] no temperature dependence (2 parameters), linear temperature dependence (4 parameter), quadratic temperature dependence (six parameter), and polynomial temperature dependence (eight parameter), respectively.

Table 6
AIC ranking and relative likelihood for candidate models for the HFC-125/[emim][TF_2N] system.

Rank	Model	*p*	AIC	Likelihood, %
1	PR-3A	3	−173.395	100
2	SRK-3A	3	−173.139	88.0
3	PR-4	4	−171.466	38.1
4	SRK-2	2	−171.422	37.3
5	SRK-4	4	−171.140	32.4
6	SRK-3B	3	−170.412	22.5
7	SRK-6	6	−168.677	9.45
8	PR-6	6	−168.626	9.22
9	SRK-8	8	−165.616	2.05
10	PR-8	8	−165.580	2.01
11	PR-3B	3	−161.691	0.287
12	PR-2	2	−160.703	0.175
13	PR-1A	1	−147.959	3E−4
14	SRK-1A	1	−140.520	$O(10^{-7})$
15	PR-1B	1	−78.484	$O(10^{-7})$
16	SRK-1B	1	−42.354	$O(10^{-7})$

other HFC/IL systems, the one parameter models have essentially zero likelihood of being able to reproduce the data.

The HFC-125/[emim][TF_2N] system again highlights the trade-off between model fit and parsimony. Although the four, six, and eight parameter models have lower MSEs than the two and three parameter models, their MSE values are not sufficiently low enough to compensate for their larger number of parameters, i.e., higher complexity, so the more parsimonious three parameter models are ranked higher. Additionally, we note the significant difference in relative likelihoods between the top two models for this system, PR-3 A (100%) and SRK-3 A (88.0%), and the model ranked third, PR-4 (38.1%). PR-3 A and SRK-3 A are more than twice as likely than PR-4 to reproduce the data, emphasizing their accuracy (MSE of 3.68E−6 MPa^2 and 3.71E−6 MPa^2, respectively, compared to the MSE of PR-4 of 3.67E−6 MPa^2). The HFC-125/[emim][TF_2N] system has the highest MSE values of all the HFC/IL systems and does not justify the larger number of parameters. Conversely, the HFC-32 systems have low enough MSEs to justify the number of parameters using AIC. The differences in MSE between the HFC-32 and HFC-125 systems explains the significant differences in AIC model ranking results.

HFC-32/[bmim][PF_6]

Table 7 shows there are six models with a relative likelihood greater than $O(10^{-1})$ for the HFC-32/[bmim][PF_6] system. The top six models are: SRK-8 (likelihood: 100%); PR-6 (likelihood: 72.2%); SRK-6 (likelihood: 58.5%); PR-8 (likelihood: 57.4%); PR-4 (likelihood: 0.244%); and SRK-4 (likelihood: 0.132%). Models with four or fewer parameters have relative likelihoods of near zero. Unlike the other two systems, the most likely model for the HFC-32/[bmim][PF_6] system is SRK-8,

Table 7
AIC ranking and relative likelihood for candidate models for the HFC-32/[bmim][PF_6] system.

Rank	Model	p	AIC	Likelihood, %
1	SRK-8	8	−172.671	100
2	PR-6	6	−172.018	72.2
3	SRK-6	6	−171.600	58.5
4	PR-8	8	−171.560	57.5
5	PR-4	4	−160.642	0.244
6	SRK-4	4	−159.405	0.132
7	PR-3A	3	−150.811	1.79×10^{-3}
8	SRK-3A	3	−149.736	1.05×10^{-3}
9	PR-2	2	−143.503	$O(10^{-7})$
10	PR-3B	3	−142.548	$O(10^{-7})$
11	SRK-2	2	−135.588	$O(10^{-7})$
12	SRK-3B	3	−132.217	$O(10^{-7})$
13	PR-1A	1	−122.272	$O(10^{-7})$
14	SRK-1A	1	−114.748	$O(10^{-7})$
15	PR-1B	1	−25.280	$O(10^{-7})$
16	SRK-1B	1	−8.909	$O(10^{-7})$

the model with the most parameters. The low AIC score indicates the improvement in MSE outweighed the complexity of regressing eight parameters. In contrast, although PR-8 had the next lowest MSE value of all the models, its MSE was not sufficiently low enough to balance its eight parameters and was ranked fourth.

Discussion

This AIC ranking analysis, comprising Step 3 of Fig. 1, leads to three key observations:

- The AIC rankings show that thermodynamic model temperature dependence is preferred in all HFC/IL systems, indicating the importance of gathering data at multiple temperatures.
- The AIC rankings show different thermodynamic models have higher likelihoods of reproducing the data for each HFC/IL system, indicating that there is not one thermodynamic model that is best for all HFC/IL systems.
- AIC provides insight as to whether a model is overfit, which is overlooked with visualization and error metrics (Step 2) alone.

The best fit parameters for the top AIC-ranked model for each system are shown in SI Table S1.

4.3. FIM analyses evaluate a model's physical interpretability

The FIMs for each of the sixteen models for the HFC-32/[emim][TF_2N] system are reported in the SI. The FIMs were scaled by Eq. (14) and computed using $\sigma_\epsilon = 0.0008$ MPa, which was also used in Morais et al. [61] and was verified by analysis of the model residuals. Each model's condition number for the HFC-32/[emim][TF_2N] system is reported in Table 8; the optimality criteria can be seen in SI Table S2. This analysis is limited to the HFC-32/[emim][TF_2N] for conciseness but can be applied to the other systems.

We observe that the four, six, and eight parameter models have condition numbers above $O(10^3)$, indicating these are sloppy models [105]. The eigendecomposition of PR-6, the top AIC ranked model for the HFC-32/[emim][TF_2N] system, is shown in Table 9. The PR-6 model has two small eigenvalues, 1.34×10^4 and 1.28×10^2, and another eigenvalue, 3.32×10^5, that are more than three orders of magnitude smaller than the largest eigenvalue. Evaluation of the corresponding eigenvectors shows that the largest direction of sloppiness arises from the $k_{ji,B}$, $k_{ij,C}$, and $k_{ji,C}$ parameters, which are part of the higher order temperature dependent terms. This suggests that these regressed parameters are highly correlated and most likely to be influenced by experimental noise and have high uncertainty. The correlation matrices reported in the Supporting Information confirm a strong (anti)correlation between pairwise combinations of $k_{ij,A}$, $k_{ij,B}$, and $k_{ij,C}$ as well as pairs of $k_{ji,A}$, $k_{ji,B}$, and $k_{ji,C}$, which complicates the physical interpretability of the parameter estimates. Moreover, we note the discrepancy between AIC-based thermodynamic model ranking and selection and parameter identifiability analysis results. Although AIC provides information on whether a model's fit justifies its complexity (number of parameters), it does not quantify the correlation between parameters as seen by examining the FIM.

Table 8
Condition number of the Fisher information matrices (FIMs) for each candidate model i for the HFC-32/[emim][TF_2N] system. The FIM of a one parameter model is a scalar on which eigendecomposition is not informative. Recall, the number of parameters in a given model corresponds with the model's name (e.g., PR-6 is a six parameter model).

Model	Condition number
PR-1A	–
SRK-1A	–
PR-1B	–
SRK-1B	–
PR-2	2.76×10^1
SRK-2	9.02×10^0
PR-3A	2.88×10^3
SRK-3A	2.89×10^3
PR-3B	1.67×10^3
SRK-3B	9.89×10^2
PR-4	1.48×10^4
SRK-4	1.59×10^4
PR-6	2.72×10^8
SRK-6	1.74×10^9
PR-8	3.43×10^{14}
SRK-8	1.75×10^{12}

Thus, Step 4 of Fig. 1 provides another insight: FIM analyses provide information on the interpretability of these chosen model parameters, i.e., whether the chosen parameters and the model function form are justified by the data.

4.4. MBDoE analyses optimize future data generation efforts

Fig. 3a shows the minimum set of experiments that are necessary to regress the top AIC ranked PR-6 model for the HFC-32/[emim][TF_2N] system. As expected, we observe the determinant is zero with fewer than six experiments. This is because calibrating a six parameter model requires at least six experiments. Moreover, the determinant increases as measurements are added and begins to reach a plateau at twenty experiments. The determinant remains $O(10^1)$ in Fig. 3a after approximately ten experimental data points, indicating that the ten best experiments contain the majority of the information needed to accurately calibrate the PR-6 model. This implies that ten experiments provide essentially the same amount of information as the original full data set (twenty-seven observations). While this is a retrospective analysis, we emphasize that this is informative for future data generating efforts.

Fig. 3b identifies the most valuable and informative experiments in the original data set. The six measurements with the most information are shown as dots in Fig. 3b: 283 K, 44.8 mol% HFC-32, 0.4 MPa; 283 K, 78.6 mol% HFC-32, 0.85 MPa; 298 K, 64.3 mol% HFC-32, 1.0 MPa; 323 K, 41.7 mol% HFC-32, 1.0 MPa; 348 K, 17.5 mol% HFC-32, 0.55 MPa; and 348 K, 28.8 mol% HFC-32, 1.0 MPa. Note these are measurements at the extreme values of the available data: there are two data points at mid-range and high pressures at the highest and lowest experimental temperature and an additional two data points at the highest pressures and compositions at the two middle temperatures. Thermodynamic models interpolate between the extremes of the data (between the temperature ranges), making the intermediate data less

Table 9
The FIM eigendecomposition of the top AIC ranked PR-6 model for the HFC-32/[emim][TF_2N] system.

Eigenvalue	Eigenvector					
–	$k_{ij,A}$	$k_{ji,A}$	$k_{ij,B}$	$k_{ji,B}$	$k_{ij,C}$	$k_{ji,C}$
3.49×10^{10}	0.4510	0.1527	0.7371	−0.04012	0.4767	0.03248
4.07×10^{8}	−0.1044	−0.7464	0.1724	0.5616	0.09957	0.2773
2.07×10^{7}	0.8290	−0.1648	−0.1386	0.08606	−0.5075	−0.03739
3.32×10^{5}	−0.07748	−0.5045	0.1762	−0.3609	−0.01606	**−0.7602**
1.34×10^{4}	0.2995	−0.2163	−0.5942	−0.1978	**0.6843**	0.05479
1.28×10^{2}	−0.05151	−0.3017	0.1536	**−0.7115**	−0.1917	0.5829

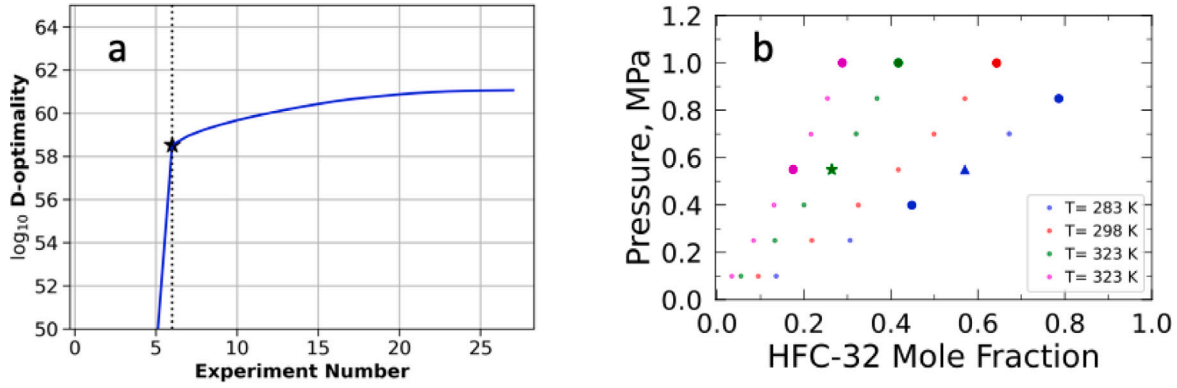

Fig. 3. Individual measurement information content analysis for the PR-6 model for the HFC-32/[emim][TF_2N] system. **Plot (a)** shows the change in the D-optimality criteria as experimental data is added to the model training set. **Plot (b)** shows the experimental solubility data for the HFC-32/[emim][TF_2N] used in this system [127]. The bold dots show the first six recommended experiments, the bold star shows the seventh recommended experiment, and the triangle shows the eighth recommended experiment.

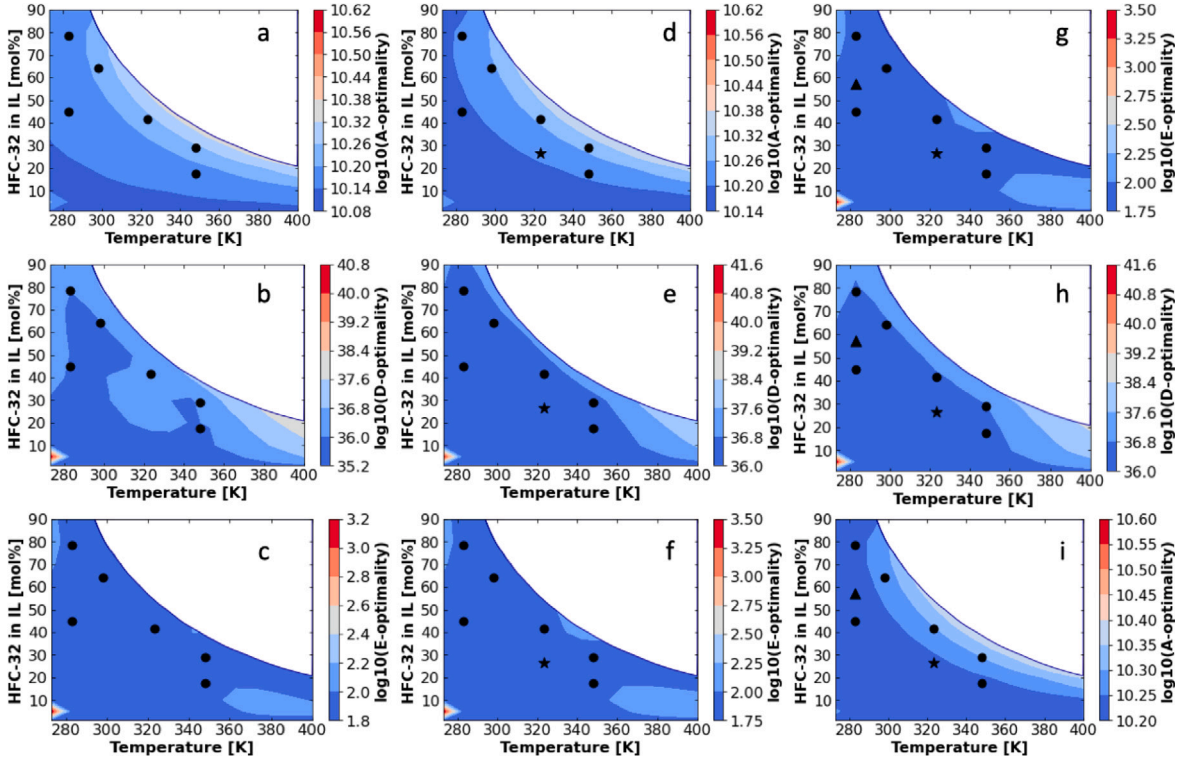

Fig. 4. A-, D-, and E-optimality criteria of measurement design space for the HFC-32/[emim][TF_2N] system using the PR-6 model after the best six data points, shown as dots (a, b, c), top seven data points (d, e, f), and eight data points (g, h, i) are added. The stars and triangles mark the seventh and eight best experiments, respectively.

informative. The seventh and eighth most informative data points occur at 323 K, 26.4 mol% HFC-32, 0.55 MPa (X) and 283 K, 57.0 mol% HFC-32, and 0.55 MPa (square). This indicates additional measurements at the temperature measurement range boundaries are useful. The additional measurement at a mid-range temperature, composition, or pressure likely provides more insight into the model's prediction of the isotherm's curvature. Fig. 4 shows the changes in the DoE metrics as these most informative six, seven, and eight experiments are added to the FIM calculation. Fig. 4 emphasizes mid-to-high pressure and composition measurements contain the most information across all temperatures, verifying the suggested locations of the seventh and eighth most valuable experiments. Recall these results assume a constant variance for the measurement error and as such measurements at higher pressures have a better signal-to-noise ratio. An alternate error structure, such as percent error, may result in different findings about the most valuable measurement.

Finally, we considered MBDoE for model discrimination. The maximum difference between pressure predictions for the HFC-32/[emim][TF_2N] systems of the first and second AIC-ranked models, PR-6 and SRK-6, respectively, occur at 71.0 mol% HFC-32 and 273 K, as determined by Eq. (15). This reinforces the insights gained from Figs. 3 and 4: data at the extremes of available experimental conditions, e.g., high pressures and mole fractions, contain more information than those at low or midduel pressures and mole fractions. For this analysis, measurement design space was expanded beyond the ranges of the current data set to encompass temperatures ranging from 273–360K, which are the extremes of currently accessible experimental conditions [61,62]. This result is confirmed by Fig. 2 which showed that the models consistently performed worse at low temperatures and high HFC-32 mole fractions; adding measurements at these conditions will show which model is better able to capture solubility phenomena at these conditions.

MBDoE analyses, comprising Step 5 of Fig. 1, provide the following insights:

- For PR-6, ten optimally selected experiments contain a majority of the information. This suggests the minimum number of necessary experiments is only a few more than the number of parameters.
- Experimental data should be collected at the extremes of accessible measurement design space.
- MBDoE metrics guide where additional measurement should be obtained in measurement design space.

These insights help optimize future laboratory experiments or molecular simulations. We note that obtaining data at the extremes of available measurement design space may be challenging or impossible using currently available data collection setups. This may motivate new advancements in instrumentation to expand the limits of thermodynamic model understanding.

5. Conclusion

We present a data science framework for rigorous thermodynamic model selection and analysis. We consider HFC/IL systems for which there are no prior studies on systematic model selection or experiment optimization. From this case study, we learn three key general recommendations widely applicable to thermodynamic modeling. First, visualization alone is not useful for model selection. Next, MSE, AIC, and identifiability analyses must be used in concert to evaluate a model's accuracy, predictive capability, and interpretability. Finally, MBDoE analyses can provide data generation recommendations that could significantly improve the efficient use of data generation resources.

We gained additional insights about thermodynamic modeling decisions for HFC/IL systems, which suggest new thermodynamic model selection and data generating protocols. Current practices emphasize measuring full solubility isotherms at a single temperature and then using the data with the most convenient thermodynamic model in AspenPlus [61,62,68]. However, we observed that HFC/IL systems favor temperature dependence in the thermodynamic model, meaning that HFC/IL thermophysical data must be obtained at multiple temperatures. We also show that there is not a "one size fits all" thermodynamic model for HFC/IL systems as the top AIC-ranked models were the PR-6, PR-3 A, and SRK-8 models for the HFC-32/[emim][TF_2N], HFC-125/[emim][TF_2N], and HFC-32/[bmim][PF_6] systems, respectively. Instead, we provide a systematic selection of the best SRK or PR thermodynamic model for each system and report the estimated parameters with uncertainty. We recommend using these models for process design and scale-up. Finally, we provided recommendations for how HFC/IL thermophysical data generating collaborators can most efficiently obtain data and that the most informative HFC/IL data is found at the measurement extremes (e.g., highest and lowest temperatures, pressures, and compositions).

These findings open new questions for data generators and thermodynamic modelers:

- How does the end use of a thermodynamic model, e.g., molecular insights or engineering design, inform the acceptable uncertainty and efforts to minimize data requirements?
- How does the finding that most informative data are at measurement bounds inform the design of new experimental or simulation techniques?
- How can we best incorporate this thermodynamic model selection and analysis workflow within a CAM/PD framework?

We emphasize these considerations are important for HFC/IL systems but are also likely to be insightful for most multiscale separation engineering endeavors.

CRediT authorship contribution statement

Bridgette J. Befort: Conceptualization, Methodology, Software, Validation, Formal analysis, Investigation, Data curation, Writing – original draft, Writing – review & editing, Visualization. **Alejandro Garciadiego:** Methodology, Software, Validation, Investigation, Writing – review & editing. **Jialu Wang:** Software, Investigation, Visualization. **Ke Wang:** Software, Investigation, Visualization. **Gabriela Franco:** Investigation, Data curation. **Edward J. Maginn:** Conceptualization, Writing – review & editing, Funding acquisition. **Alexander W. Dowling:** Conceptualization, Methodology, Software, Formal analysis, Writing – original draft, Writing – review & editing, Supervision, Project administration, Funding acquisition.

Declaration of competing interest

The authors declare that they have no known competing financial interests or personal relationships that could have appeared to influence the work reported in this paper.

Data availability

Data and software available online for free at https://github.com/dowlinglab/HFC-IL-thermodynamic-model-selection.

Acknowledgments

B.J.B., A.W.D., and E.J.M. acknowledge funding from the National Science Foundation, Award number CBET-1917474. B.J.B. acknowledges funding from the Richard and Peggy Notebaert Premier Fellowship.

Appendix A

Table 10
Description of abbreviations utilized.

Abbreviation	Expansion
AIC	Akaike information criteria
CAM/PD	Computer-aided molecular and process design
DoE	Design of experiments
EoS	Equation of state
FIM	Fischer information matrix
GWP	Global warming potential
HFC	Hydrofluorocarbon
IDAES	Institute for the Design of Advanced Energy Systems
IL	Ionic liquid
MBDoE	Model-based design of experiments
MC	Monte Carlo
MSE	Mean squared error
NRTL	Non-random two liquid
PR	Peng–Robinson
RK	Redlick–Kwong
SAFT	Statistical associating fluid theory
SRK	Soave–Redlich–Kwong
vdW	van der Waals

Appendix B. Supplementary data

Supplementary material related to this article can be found online at https://doi.org/10.1016/j.fluid.2023.113833.

PDF document describes the multistart initialization procedures and reports additional results for the HFC-125/[emim][TF_2N] and HFC-32/[bmim][PF_6] systems. Excel spreadsheet reports the fitted parameters, Fisher information matrices, correlation matrices, and eigendecompositions for the studied models and systems.

References

[1] M. Ko, R. Shia, N. Sze., H. Magid, R.G. Bray, Atmospheric lifetime and global warming potential of HFC-245fa, J. Geophys. Res. 104 (D7) (1999) 8173–8181.

[2] C. Clerbaux, R. Colin, P.C. Simon, C. Granier, Infrared cross sections and global warming potentials of 10 alternative hydrohalocarbon, J. Geophys. Res. 98 (D6) (1993) 10,491–10,497, http://dx.doi.org/10.1029/93JD00390.

[3] Y. Xu, D. Zaelke, G.J.M. Velders, V. Ramanathan, The role of HFCs in mitigating 21st century climate change, Atmos. Chem. Phys. 13 (12) (2013) 6083–6089, http://dx.doi.org/10.5194/acp-13-6083-2013.

[4] Y. Xu, D. Zaelke, G.J. Velders, V. Ramanathan, The role of HFCs in mitigating 21st century climate change, Atmos. Chem. Phys. 13 (12) (2013) 6083–6089.

[5] Y. Heredia-Aricapa, J. Belman-Flores, A. Mota-Babiloni, J. Serrano-Arellano, J.J. García-Pabón, Overview of low GWP mixtures for the replacement of HFC refrigerants: R134a, R404A and R410A, Int. J. Refrig. 111 (2020) 113–123.

[6] M.O. McLinden, M.L. Huber, (R) evolution of refrigerants, J. Chem. Eng. Data 65 (9) (2020) 4176–4193.

[7] EPA, Phasedown of hydrofluorocarbons: Establishing the allowance allocation and trading program under the American innovation and manufacturing act, 2022, (Accessed 23 July 2022).

[8] EPA, Draft regulatory impact analysis for phasing down production and consumption of hydrofluorocarbons HFCs, 2022, (Accessed 23 July 2022).

[9] UN, Montreal protocol 1989, 2022, URL https://ozone.unep.org/treaties/montreal-protocoll. (Accessed 23 July 2022).

[10] UN, Amendment to the montreal protocol on substances that deplete the ozone layer, 2022, (Accessed 23 July 2022).

[11] U.N.E. Programme, GWP-ODP Calculator, United National Environment Programme: http://web.unep.org/ozonaction/resources/gwp-odp-calculator.

[12] Daikin, 32 Reasons why R-32 is the right answer, 2022, (Accessed 23 July 2022).

[13] P. Purohit, L. Höglund-Isaksson, J. Dulac, N. Shah, M. Wei, P. Rafaj, W. Schöpp, Electricity savings and greenhouse gas emission reductions from global phase-down of hydrofluorocarbons, Atmos. Chem. Phys. 20 (19) (2020) 11305–11327.

[14] C.G. Albá, I.I. Alkhatib, F. Llovell, L.F. Vega, Assessment of low global warming potential refrigerants for drop-in replacement by connecting their molecular features to their performance, ACS Sustain. Chem. Eng. 9 (50) (2021) 17034–17048.

[15] J.S. Brown, HFOs new, low global warming potential refrigerants, ASHRAE J. 51 (8) (2009) 22–29.

[16] M.O. McLinden, C.J. Seeton, A. Pearson, New refrigerants and system configurations for vapor-compression refrigeration, Science 370 (6518) (2020) 791–796.

[17] A.S. Alshehri, A.K. Tula, F. You, R. Gani, Next generation pure component property estimation models: With and without machine learning techniques, AIChE J. 68 (6) (2022) e17469.

[18] D. Jovell, R. Gonzalez-Olmos, F. Llovell, A computational drop-in assessment of hydrofluoroethers in Organic Rankine Cycles, Energy (2022) 124319.

[19] D. Jovell, J.O. Pou, F. Llovell, R. Gonzalez-Olmos, Life cycle assessment of the separation and recycling of fluorinated gases using ionic liquids in a circular economy framework, ACS Sustain. Chem. Eng. 10 (1) (2021) 71–80.

[20] J.J. McKetta, Unit Operations Handbook, CRC Press, 1992.

[21] Z. Lei, B. Chen, Z. Ding, Special Distillation Processes, Elsevier Science, Amsterdam, 2005, pp. 145–177, http://dx.doi.org/10.1016/B978-044451648-0/50003-3.

[22] M. Shiflett, A. Yokozeki, Separation of difluoromethane and pentafluoroethane by extractive distillation using ionic liquid, Chim. Oggi-Chem. Today 24 (2006) 28–30.

[23] A.D. Yancey, S.J. Terian, B.J. Shaw, T.M. Bish, D.R. Corbin, M.B. Shiflett, A review of fluorocarbon sorption on porous materials, Microporous Mesop. Mater. (2021) 111654.

[24] A.D. Yancey, D.R. Corbin, M.B. Shiflett, Difluoromethane (HFC-32) and pentafluoroethane (HFC-125) sorption on linde type A (LTA) zeolites for the separation of azeotropic hydrofluorocarbon refrigerant mixtures, Langmuir 38 (6) (2022) 1937–1953.

[25] D.K. Wanigarathna, J. Gao, B. Liu, Metal organic frameworks for adsorption-based separation of fluorocompounds: A review, Mater. Adv. 1 (3) (2020) 310–320.

[26] Y.-Y. Xiong, R. Krishna, T. Pham, K.A. Forrest, C.-X. Chen, Z.-W. Wei, J.-J. Jiang, H.-P. Wang, Y. Fan, M. Pan, et al., Pore-nanospace engineering of mixed-ligand metal–organic frameworks for high adsorption of hydrofluorocarbons and hydrochlorofluorocarbons, Chem. Mater. (2022).

[27] J.M. Asensio-Delgado, S. Asensio-Delgado, G. Zarca, A. Urtiaga, Analysis of hybrid compression absorption refrigeration using low-GWP HFC or HFO/ionic liquid working pairs, Int. J. Refrig. 134 (2022) 232–241.

[28] T. Jiang, X. Meng, Y. Sun, L. Jin, Q. Wei, J. Wang, X. Wang, M. He, Absorption behavior for R1234ze (E) and R1233zd (E) in [P66614][Cl] as working fluids in absorption refrigeration systems, Int. J. Refrig. 131 (2021) 178–185.

[29] A.N. Harders, E.R. Sturd, J.E. Vallier, D.R. Corbin, W.R. White, C.P. Junk, M.B. Shiflett, Selective separation of HFC-32 from R-410A using poly (dimethylsiloxane) and a copolymer of perfluoro (butenyl vinyl ether) and perfluoro (2, 2-dimethyl-1, 3-dioxole), J. Membr. Sci. 652 (2022) 120467.

[30] C. Hermida-Merino, F. Pardo, G. Zarca, J.M. Araújo, A. Urtiaga, M.M. Piñeiro, A.B. Pereiro, Integration of stable ionic liquid-based nanofluids into polymer membranes. Part I: membrane synthesis and characterization, Nanomaterials 11 (3) (2021) 607.

[31] F. Pardo, S.V. Gutiérrez-Hernández, C. Hermida-Merino, J.M. Araújo, M.M. Piñeiro, A.B. Pereiro, G. Zarca, A. Urtiaga, Integration of stable ionic liquid-based nanofluids into polymer membranes. Part II: gas separation properties toward fluorinated greenhouse gases, Nanomaterials 11 (3) (2021) 582.

[32] F. Pardo, S.V. Gutiérrez-Hernández, G. Zarca, A. Urtiaga, Toward the recycling of low-GWP hydrofluorocarbon/hydrofluoroolefin refrigerant mixtures using composite ionic liquid–polymer membranes, ACS Sustain. Chem. Eng. 9 (20) (2021) 7012–7021.

[33] F. Pardo, G. Zarca, A. Urtiaga, Separation of refrigerant gas mixtures containing R32, R134a, and R1234yf through poly (ether-block-amide) membranes, ACS Sustain. Chem. Eng. 8 (6) (2020) 2548–2556.

[34] S. Asensio-Delgado, F. Pardo, G. Zarca, A. Urtiaga, Absorption separation of fluorinated refrigerant gases with ionic liquids: Equilibrium, mass transport, and process design, Sep. Purif. Technol. 276 (2021) 119363.

[35] K. Marsh, J. Boxall, R. Lichtenthaler, Room temperature ionic liquids and their mixtures–A review, Fluid Phase Equilib. 219 (1) (2004) 93–98, http://dx.doi.org/10.1016/j.fluid.2004.02.003, Molecular Thermodynamics and Molecular Simulation.

[36] Y. Zhao, R. Gani, R.M. Afzal, X. Zhang, S. Zhang, Ionic liquids for absorption and separation of gases: An extensive database and a systematic screening method, AIChE J. 63 (4) (2017) 1353–1367, http://dx.doi.org/10.1002/aic.15618.

[37] C. Jork, M. Seiler, Y.-A. Beste, W. Arlt, Influence of ionic liquids on the phase behavior of aqueous azeotropic systems, J. Chem. Eng. Data 49 (4) (2004) 852–857, http://dx.doi.org/10.1021/je034183r.

[38] Z. Lei, C. Dai, B. Chen, Gas solubility in ionic liquids, Chem. Rev. 114 (2) (2014) 1289–1326, http://dx.doi.org/10.1021/cr300497a.

[39] M.B. Shiflett, E.J. Maginn, The solubility of gases in ionic liquids, AIChE J. 63 (11) (2017) 4722–4737.

[40] N.V. Plechkova, K.R. Seddon, Applications of ionic liquids in the chemical industry, Chem. Soc. Rev. 37 (1) (2008) 123–150.

[41] J.D. Holbrey, K.R. Seddon, The phase behaviour of 1-alkyl-3-methylimidazolium tetrafluoroborates; ionic liquids and ionic liquid crystals, J. Chem. Soc., Dalton Trans. (13) (1999) 2133–2140.

[42] A. Quaglia, C.L. Gargalo, S. Chairakwongsa, G. Sin, R. Gani, Systematic network synthesis and design: problem formulation, superstructure generation, data management and solution, Comput. Chem. Eng. 72 (2015) 68–86.

[43] S. Chai, Z. Song, T. Zhou, L. Zhang, Z. Qi, Computer-aided molecular design of solvents for chemical separation processes, Curr. Opin. Chem. Eng. 35 (2022) 100732.

[44] S. Kaiser, S. Engell, Integrating superstructure optimization under uncertainty and optimal experimental design in early stage process development, Comput. Aided Chem. Eng. 48 (2020) 799–804.

[45] A. Zunger, Inverse design in search of materials with target functionalities, Nat. Rev. Chem. 2 (4) (2018) 1–16.

[46] R. Gómez-Bombarelli, J.N. Wei, D. Duvenaud, J.M. Hernández-Lobato, B. Sánchez-Lengeling, D. Sheberla, J. Aguilera-Iparraguirre, T.D. Hirzel, R.P. Adams, A. Aspuru-Guzik, Automatic chemical design using a data-driven continuous representation of molecules, ACS Cent. Sci. 4 (2) (2018) 268–276.

[47] L.F. Fuentes-Cortés, A. Flores-Tlacuahuac, K.D. Nigam, Machine learning algorithms used in PSE environments: A didactic approach and critical perspective, Ind. Eng. Chem. Res. (2022).

[48] S.I. Sandler, Chemical, Biochemical, and Engineering Thermodynamics, John Wiley & Sons, 2017.

[49] A.W. Dowling, L.T. Biegler, A framework for efficient large scale equation-oriented flowsheet optimization, Comput. Chem. Eng. 72 (2015) 3–20.

[50] A.W. Dowling, C. Balwani, Q. Gao, L.T. Biegler, Optimization of sub-ambient separation systems with embedded cubic equation of state thermodynamic models and complementarity constraints, Comput. Chem. Eng. 81 (2015) 323–343.

[51] M.B. Shiflett, M.A. Harmer, C.P. Junk, A. Yokozeki, Solubility and diffusivity of 1, 1, 1, 2-tetrafluoroethane in room-temperature ionic liquids, Fluid Phase Equilib. 242 (2) (2006) 220–232.

[52] M.S. Monjur, A. Iftakher, M.F. Hasan, Separation process synthesis for high-GWP refrigerant mixtures: Extractive distillation using ionic liquids, Ind. Eng. Chem. Res. 61 (12) (2022) 4390–4406.

[53] S. Asensio-Delgado, M. Viar, F. Pardo, G. Zarca, A. Urtiaga, Gas solubility and diffusivity of hydrofluorocarbons and hydrofluoroolefins in cyanide-based ionic liquids for the separation of refrigerant mixtures, Fluid Phase Equilib. 549 (2021) 113210.

[54] M.B. Shiflett, A. Yokozeki, Solubilities and diffusivities of carbon dioxide in ionic liquids:[bmim][PF6] and [bmim][BF4], Ind. Eng. Chem. Res. 44 (12) (2005) 4453–4464.

[55] A. Yokozeki, M.B. Shiflett, Global phase behaviors of trifluoromethane in ionic liquid [bmim][PF6], AIChE J. 52 (11) (2006) 3952–3957.

[56] M.B. Shiflett, A. Yokozeki, Solubility differences of halocarbon isomers in ionic liquid [emim][Tf2N], J. Chem. Eng. Data 52 (5) (2007) 2007–2015.

[57] A. Yokozeki, M.B. Shiflett, Binary and ternary phase diagrams of benzene, hexafluorobenzene, and ionic liquid [emim][Tf2N] using equations of state, Ind. Eng. Chem. Res. 47 (21) (2008) 8389–8395.

[58] M.B. Shiflett, A. Yokozeki, Separation of CO2 and H2S using room-temperature ionic liquid [bmim][PF6], Fluid Phase Equilib. 294 (1–2) (2010) 105–113.

[59] M.B. Shiflett, A.M.S. Niehaus, B.A. Elliott, A. Yokozeki, Phase behavior of N2O and CO2 in room-temperature ionic liquids [bmim][Tf2N],[bmim][BF4],[bmim][N (CN) 2],[bmim][Ac],[eam][NO3], and [bmim][SCN], Int. J. Thermophys. 33 (3) (2012) 412–436.

[60] A. Yokozeki, M.B. Shiflett, Gas solubilities in ionic liquids using a generic van der Waals equation of state, J. Supercrit. Fluids 55 (2) (2010) 846–851.

[61] A.R.C. Morais, A.N. Harders, K.R. Baca, G.M. Olsen, B.J. Befort, A.W. Dowling, E.J. Maginn, M.B. Shiflett, Phase equilibria, diffusivities, and equation of state modeling of HFC-32 and HFC-125 in imidazolium-based ionic liquids for the separation of R-410A, Ind. Eng. Chem. Res. 59 (40) (2020) 18222–18235.

[62] K.R. Baca, G.M. Olsen, L. Matamoros Valenciano, M.G. Bennett, D.M. Haggard, B.J. Befort, A. Garciadiego, A.W. Dowling, E.J. Maginn, M.B. Shiflett, Phase equilibria and diffusivities of HFC-32 and HFC-125 in ionic liquids for the separation of R-410A, ACS Sustain. Chem. Eng. 10 (2) (2021) 816–830.

[63] A. Garciadiego, M. Mazumder, B.J. Befort, A.W. Dowling, Modeling and optimization of ionic liquid enabled extractive distillation of ternary azeotrope mixtures, Comput. Aided Chem. Eng. 49 (2022) 307–312.

[64] A. Garciadiego, B.J. Befort, G. Franco, M. Mazumder, A.W. Dowling, What data are most valuable to screen ionic liquid entrainers for hydrofluorocarbon refrigerant reuse and recycling? Ind. Eng. Chem. Res. 61 (2022) 18412–18425.

[65] S. Asensio-Delgado, D. Jovell, G. Zarca, A. Urtiaga, F. Llovell, Thermodynamic and process modeling of the recovery of R410A compounds with ionic liquids, Int. J. Refrig. 118 (2020) 365–375.

[66] I.I. Alkhatib, C.G. Albá, A.S. Darwish, F. Llovell, L.F. Vega, Searching for sustainable refrigerants by bridging molecular modeling with machine learning, Ind. Eng. Chem. Res. (2022).

[67] H. Qin, J. Cheng, H. Yu, T. Zhou, Z. Song, Hierarchical ionic liquid screening integrating COSMO-RS and Aspen Plus for selective recovery of hydrofluorocarbons and hydrofluoroolefins from a refrigerant blend, Ind. Eng. Chem. Res. 61 (11) (2022) 4083–4094.

[68] E.A. Finberg, M.B. Shiflett, Process designs for separating R-410A, R-404A, and R-407C using extractive distillation and ionic liquid entrainers, Ind. Eng. Chem. Res. 60 (44) (2021) 16054–16067.

[69] E.A. Finberg, T.L. May, M.B. Shiflett, Multicomponent refrigerant separation using extractive distillation with ionic liquids, Ind. Eng. Chem. Res. (2022).

[70] E.J. Maginn, From discovery to data: What must happen for molecular simulation to become a mainstream chemical engineering tool, AIChE J. 55 (6) (2009) 1304–1310.

[71] C.A. Faúndez, R.A. Campusano, J.O. Valderrama, Misleading results on the use of artificial neural networks for correlating and predicting properties of fluids. A case on the solubility of refrigerant R-32 in ionic liquids, J. Mol. Liq. 298 (2020) 112009.

[72] E.N. Fierro, C.A. Faúndez, A.S. Muñoz, Influence of thermodynamically inconsistent data on modeling the solubilities of refrigerants in ionic liquids using an artificial neural network, J. Mol. Liq. 337 (2021) 116417.

[73] S. Asensio-Delgado, F. Pardo, G. Zarca, A. Urtiaga, Machine learning for predicting the solubility of high-GWP fluorinated refrigerants in ionic liquids, J. Mol. Liq. 367 (2022) 120472.

[74] A. Yokozeki, Solubility of refrigerants in various lubricants, Int. J. Thermophys. 22 (4) (2001) 1057–1071.

[75] F.E. Pereira, E. Keskes, A. Galindo, G. Jackson, C.S. Adjiman, Integrated solvent and process design using a SAFT-VR thermodynamic description: High-pressure separation of carbon dioxide and methane, Comput. Chem. Eng. 35 (3) (2011) 474–491.

[76] C.S. Adjiman, A. Galindo, G. Jackson, Molecules matter: the expanding envelope of process design, Comput. Aided Chem. Eng. 34 (2014) 55–64.

[77] M.G. Bjørner, G. Sin, G.M. Kontogeorgis, Uncertainty analysis of the CPA and a quadrupolar CPA equation of state–With emphasis on CO_2, Fluid Phase Equilib. 414 (2016) 29–47.

[78] J.-C. De Hemptinne, J.-M. Ledanois, Select Thermodynamic Models for Process Simulation: A Practical Guide using a Three Steps Methodology, Editions Technip, 2012.

[79] J.E. Edwards, Process modelling selection of thermodynamic methods, in: UK ChemCAD Seminar, 2000.

[80] J. Haydary, Chemical Process Design and Simulation: Aspen Plus and Aspen Hysys Applications, John Wiley & Sons, 2019.

[81] S.I. Sandler, Using Aspen Plus in Thermodynamics Instruction: A Step-By-Step Guide, John Wiley & Sons, 2015.

[82] R.R. Duran, P.E. Falsetti, L. Muhr, R. Privat, D. Barth, Phase equilibrium study of the ternary system CO_2^+ H_2O^+ ethanol at elevated pressure: thermodynamic model selection. Application to supercritical extraction of polar compounds, J. Supercrit. Fluids 138 (2018) 17–28.

[83] C. Ashraf, N. Joshi, D.A. Beck, J. Pfaendtner, Data science in chemical engineering: Applications to molecular science, Annu. Rev. Chem. Biomol. Eng. 12 (1) (2021).

[84] O. Lötgering-Lin, A. Schöniger, W. Nowak, J. Gross, Bayesian model selection helps to choose objectively between thermodynamic models: a demonstration of selecting a viscosity model based on entropy scaling, Ind. Eng. Chem. Res. 55 (38) (2016) 10191–10207.

[85] T. Hastie, R. Tibshirani, J.H. Friedman, J.H. Friedman, The Elements of Statistical Learning: Data Mining, Inference, and Prediction, Vol. 2, Springer, 2009.

[86] D.A. Beck, J.M. Carothers, V.R. Subramanian, J. Pfaendtner, Data science: Accelerating innovation and discovery in chemical engineering, AIChE J. 62 (5) (2016) 1402–1416.

[87] A. Thebelt, J. Wiebe, J. Kronqvist, C. Tsay, R. Misener, Maximizing information from chemical engineering data sets: applications to machine learning, Chem. Eng. Sci. 252 (2022) 117469.

[88] E.A. Eugene, W.A. Phillip, A.W. Dowling, Data science-enabled molecular-to-systems engineering for sustainable water treatment, Curr. Opin. Chem. Eng. 26 (2019) 122–130.

[89] F. Provost, T. Fawcett, Data science and its relationship to big data and data-driven decision making, Big Data 1 (1) (2013) 51–59.

[90] V. Dhar, Data science and prediction, Commun. ACM 56 (12) (2013) 64–73.

[91] A. Lee, J.H. Ghouse, J.C. Eslick, C.D. Laird, J.D. Siirola, M.A. Zamarripa, D. Gunter, J.H. Shinn, A.W. Dowling, D. Bhattacharyya, L.T. Biegler, A.P. Burgard, D.C. Miller, The IDAES process modeling framework and model library–Flexibility for process simulation and optimization, J. Adv. Manuf. Process. 3 (3) (2021) e10095, http://dx.doi.org/10.1002/amp2.10095.

[92] M.L. Bynum, G.A. Hackebeil, W.E. Hart, C.D. Laird, B.L. Nicholson, J.D. Siirola, J.-P. Watson, D.L. Woodruff, Pyomo–Optimization Modeling in Python, Vol. 67, third ed., Springer Science & Business Media, 2021.

[93] W.E. Hart, J.-P. Watson, D.L. Woodruff, Pyomo: modeling and solving mathematical programs in Python, Math. Program. Comput. 3 (3) (2011) 219–260.

[94] S.R. Eliason, Maximum Likelihood Estimation: Logic and Practice, No. 96, Sage, 1993.

[95] Y. Bard, Nonlinear Parameter Estimation, Academic Press, 1974.

[96] M.C. Kennedy, A. O'Hagan, Bayesian calibration of computer models, J. R. Stat. Soc. Ser. B Stat. Methodol. 63 (3) (2001) 425–464.

[97] Z.-H. Lu, S.-M. Chow, E. Loken, A comparison of Bayesian and frequentist model selection methods for factor analysis models, Psychol. Methods 22 (2) (2017) 361.

[98] H. Leeb, B.M. Pötscher, Model selection and inference: Facts and fiction, Econom. Theory 21 (1) (2005) 21–59.
[99] Y. Gu, H.-L. Wei, M.M. Balikhin, Nonlinear predictive model selection and model averaging using information criteria, Syst. Sci. Control Eng. 6 (1) (2018) 319–328.
[100] S.T. Buckland, K.P. Burnham, N.H. Augustin, Model selection: an integral part of inference, Biometrics (1997) 603–618.
[101] G. Claeskens, N.L. Hjort, Model Selection and Model Averaging, Cambridge University Press, 2008.
[102] D. Hou, I. Hassan, L. Wang, Review on building energy model calibration by Bayesian inference, Renew. Sustain. Energy Rev. 143 (2021) 110930.
[103] R.A. Fisher, Design of experiments, Br. Med. J. 1 (3923) (1936) 554.
[104] D.M. Bates, D.G. Watts, Nonlinear Regression Analysis and Its Applications, Wiley, 1988.
[105] J. Wang, A.W. Dowling, Pyomo. DOE: An open-source package for model-based design of experiments in Python, AIChE J. 68 (12) (2022) e17813.
[106] G. Strang, G. Strang, G. Strang, G. Strang, Introduction to Linear Algebra, Vol. 3, Wellesley-Cambridge Press Wellesley, MA, 1993.
[107] J. Graciano, D.F. Mendoza, G.A. Le Roux, Performance comparison of parameter estimation techniques for unidentifiable models, Comput. Chem. Eng. 64 (2014) 24–40.
[108] A. Raue, C. Kreutz, T. Maiwald, J. Bachmann, M. Schilling, U. Klingmüller, J. Timmer, Structural and practical identifiability analysis of partially observed dynamical models by exploiting the profile likelihood, Bioinformatics 25 (15) (2009) 1923–1929.
[109] O.-T. Chis, A.F. Villaverde, J.R. Banga, E. Balsa-Canto, On the relationship between sloppiness and identifiability, Math. Biosci. 282 (2016) 147–161.
[110] R.N. Gutenkunst, F.P. Casey, J.J. Waterfall, C.R. Myers, J.P. Sethna, Extracting falsifiable predictions from sloppy models, Ann. New York Acad. Sci. 1115 (1) (2007) 203–211.
[111] B.J. Befort, R.S. DeFever, G.M. Tow, A.W. Dowling, E.J. Maginn, Machine learning directed optimization of classical molecular modeling force fields, J. Chem. Inform. Model. 61 (9) (2021) 4400–4414.
[112] K. Ghosh, S. Vernuccio, A.W. Dowling, Nonlinear reactor design optimization with embedded microkinetic model information, Front. Chem. Eng. 4 (2022) 898685.
[113] W. Whiting, V. Vasquez, M. Meerschaert, Techniques for assessing the effects of uncertainties in thermodynamic models and data, Fluid Phase Equilib. 158 (1999) 627–641.
[114] S. Hajipour, M.A. Satyro, Uncertainty analysis applied to thermodynamic models and process design–1. Pure components, Fluid Phase Equilib. 307 (1) (2011) 78–94.
[115] S. Hajipour, M.A. Satyro, M.W. Foley, Uncertainty analysis applied to thermodynamic models and process design–2. Binary mixtures, Fluid Phase Equilib. 364 (2014) 15–30.
[116] V.R. Vasquez, W.B. Whiting, Effect of data type on thermodynamic model parameter estimation: A Monte Carlo approach, Ind. Eng. Chem. Res. 37 (3) (1998) 1122–1129.
[117] H. Cheung, J. Frutiger, I.H. Bell, J. Abildskov, G. Sin, S. Wang, Covariance-based uncertainty analysis of reference equations of state, J. Chem. Eng. Data 65 (2) (2020) 503–522.
[118] K. Wang, M. Zeng, J. Wang, W. Shang, Y. Zhang, T. Luo, A.W. Dowling, When physics-informed data analytics outperforms black-box machine learning: A case study in thickness control for additive manufacturing, Digit. Chem. Eng. 6 (2023) 100076.
[119] W.G. Hunter, A.M. Reiner, Designs for discriminating between two rival models, Technometrics 7 (3) (1965) 307–323.
[120] G. Buzzi-Ferraris, P. Forzatti, A new sequential experimental design procedure for discriminating among rival models, Chem. Eng. Sci. 38 (2) (1983) 225–232.
[121] G.B. Ferraris, P. Forzatti, G. Emig, H. Hofmann, Sequential experimental design for model discrimination in the case of multiple responses, Chem. Eng. Sci. 39 (1) (1984) 81–85.
[122] A.L. Alberton, M. Schwaab, M.W.N. Lobão, J.C. Pinto, Experimental design for the joint model discrimination and precise parameter estimation through information measures, Chem. Eng. Sci. 66 (9) (2011) 1940–1952.
[123] F. Galvanin, E. Cao, N. Al-Rifai, V. Dua, A. Gavriilidis, Optimal design of experiments for the identification of kinetic models of methanol oxidation over silver catalyst, Chim. Oggi-Chem. Today 33 (3) (2015) 51–56.
[124] F. Galvanin, E. Cao, N. Al-Rifai, A. Gavriilidis, V. Dua, A joint model-based experimental design approach for the identification of kinetic models in continuous flow laboratory reactors, Comput. Chem. Eng. 95 (2016) 202–215.
[125] A. Pankajakshan, C. Waldron, M. Quaglio, A. Gavriilidis, F. Galvanin, A multi-objective optimal experimental design framework for enhancing the efficiency of online model identification platforms, Engineering 5 (6) (2019) 1049–1059.
[126] M. Schwaab, F.M. Silva, C.A. Queipo, A.G. Barreto Jr., M. Nele, J.C. Pinto, A new approach for sequential experimental design for model discrimination, Chem. Eng. Sci. 61 (17) (2006) 5791–5806.
[127] M.B. Shiflett, M.A. Harmer, C.P. Junk, A. Yokozeki, Solubility and diffusivity of difluoromethane in room-temperature ionic liquids, J. Chem. Eng. Data 51 (2) (2006) 483–495.
[128] M.B. Shiflett, A. Yokozeki, Binary vapor–liquid and vapor–liquid–liquid equilibria of hydrofluorocarbons (HFC-125 and HFC-143a) and hydrofluoroethers (HFE-125 and HFE-143a) with ionic liquid [emim][Tf2N], J. Chem. Eng. Data 53 (2) (2008) 492–497.
[129] M.B. Shiflett, A. Yokozeki, Solubility and diffusivity of hydrofluorocarbons in room-temperature ionic liquids, AIChE J. 52 (3) (2006) 1205–1219.
[130] E.W. Lemmon, M.L. Huber, M.O. McLinden, NIST reference fluid thermodynamic and transport properties–REFPROP, in: NIST Standard Reference Database, Vol. 23, 2002, p. v7.
[131] C.-Y. Gau, J.F. Brennecke, M.A. Stadtherr, Reliable nonlinear parameter estimation in VLE modeling, Fluid Phase Equilib. 168 (1) (2000) 1–18.
[132] J. Höller, P. Bickert, P. Schwartz, M. von Kurnatowski, J. Kerber, N. Künzle, H.-M. Lorenz, N. Asprion, S. Blagov, M. Bortz, Parameter estimation strategies in thermodynamics, ChemEngineering 3 (2) (2019) 56.
[133] A. Costa, F. da Silva, F. Pessoa, Parameter estimation of thermodynamic models for high-pressure systems employing a stochastic method of global optimization, Braz. J. Chem. Eng. 17 (2000) 349–354.
[134] W.R. Esposito, C.A. Floudas, Parameter estimation in nonlinear algebraic models via global optimization, Comput. Chem. Eng. 22 (1998) S213–S220.
[135] S. Amaran, N.V. Sahinidis, Global optimization of nonlinear least-squares problems by branch-and-bound and optimality constraints, Top 20 (1) (2012) 154–172.
[136] N.V. Sahinidis, BARON: A general purpose global optimization software package, J. Global Optim. 8 (2) (1996) 201–205.
[137] B.E. Poling, J.M. Prausnitz, J.P. O'Connell, Properties of Gases and Liquids, fifth ed., McGraw-Hill Education, New York, Chicago, San Francisco, Athens, London, Madrid, Mexico City, Milan, New Delhi, Singapore, Sydney, Toronto, 2001, p. 120.
[138] L.P. Rebelo, J.N. Canongia Lopes, J.M. Esperança, E. Filipe, On the critical temperature, normal boiling point, and vapor pressure of ionic liquids, J. Phys. Chem. B 109 (13) (2005) 6040–6043.
[139] N. Rai, E.J. Maginn, Critical behaviour and vapour-liquid coexistence of 1-alkyl-3-methylimidazolium bis (trifluoromethylsulfonyl) amide ionic liquids via Monte Carlo simulations, Faraday Discuss. 154 (2012) 53–69.
[140] R. Privat, J.-N. Jaubert, The state of the art of cubic equations of state with temperature-dependent binary interaction coefficients: From correlation to prediction, Fluid Phase Equilib. (2022) 113697.
[141] A. Wächter, L.T. Biegler, On the implementation of a primal-dual interior point filter line search algorithm for large-scale nonlinear programming, Math. Program. 106 (1) (2007) 25–57.
[142] HSL, A collection of Fortran codes for large scale scientific computation, 2021, URL http://www.hsl.rl.ac.uk/. (Accessed 6 January 2021).